



HAL
open science

Characterization of fouling protein deposits under the effect of shear by observation with a scanning electron microscope

Msibi Zanélé Paméla

► **To cite this version:**

Msibi Zanélé Paméla. Characterization of fouling protein deposits under the effect of shear by observation with a scanning electron microscope. Food engineering. 2023. hal-04174887

HAL Id: hal-04174887

<https://hal.inrae.fr/hal-04174887v1>

Submitted on 1 Aug 2023

HAL is a multi-disciplinary open access archive for the deposit and dissemination of scientific research documents, whether they are published or not. The documents may come from teaching and research institutions in France or abroad, or from public or private research centers.

L'archive ouverte pluridisciplinaire **HAL**, est destinée au dépôt et à la diffusion de documents scientifiques de niveau recherche, publiés ou non, émanant des établissements d'enseignement et de recherche français ou étrangers, des laboratoires publics ou privés.



Distributed under a Creative Commons Attribution - NonCommercial - NoDerivatives 4.0 International License

INRAE



CHARACTERIZATION OF FOULING PROTEIN DEPOSITS UNDER THE EFFECT OF SHEAR BY OBSERVATION WITH A SCANNING ELECTRON MICROSCOPE

M2 Internship Report by MSIBI Zanele Pamela



Supervisor: Dr. LANOTTE Luca

Co-Supervisor: Dr. LEE Jeehyun

02 - 02 - 2023 to 31- 07 - 2023

Abstract

Fouling in the dairy industry is one of the major detrimental issues that develop during concentration by evaporation. Fouling is characterized by a layer of the product embedded on the internal surface where the product flows. Fouling has been reported to compromise product quality and diminish the efficiency of industrial operations. Product composition and process parameters have been studied to understand fouling. It has been discovered that whey proteinous material, particularly, whey proteins in dairy products are linked to fouling, with the coupled effect of process parameters. Our hypothesis is that the shear rate that reigns in the evaporators could be responsible for fouling. While several studies have investigated the shear effect of the denaturation and aggregation of whey proteins, it remains unclear what occurs in the surface material due to the contradicting discoveries. To fulfill this gap, the influence of shear on whey protein denaturation and aggregation was studied at a fixed partial denaturation temperature (65°C). Whey protein solutions were prepared to a concentration of 5% *wt* and 10% *wt* and individually underwent a shear treatment by rheometry - parallel plate geometry. The shear treatment was performed at varied shear rates from 0s⁻¹ to 200s⁻¹. The morphology of the aggregates was studied for qualitative characteristics: size distribution, shape, and structure, under scanning electron microscopy, as a function of shear rate and protein concentration. Results revealed that the increase in shear rate facilitated aggregate growth at 5% *wt* WPI, while it inhibited the growth when shear rates were increased 140 - 200s⁻¹ at 10% *wt*. An increase in shear rate up to 200 s⁻¹ and protein concentration from 5% - 10% *wt* WPI reduced aggregate porosity.

Keywords: Concentration by vaporation, Whey proteins, Shear rate, Aggregate, Morphology, denaturation

Résumé

L'encrassement dans l'industrie laitière est l'un des principaux problèmes qui se posent lors de la concentration par évaporation. L'encrassement se caractérise par une couche de produit incrustée sur la surface interne où le produit s'écoule. L'encrassement compromet la qualité du produit et réduit l'efficacité des opérations industrielles. La composition du produit et les paramètres du processus ont été étudiés pour comprendre l'encrassement. On a découvert que les matières protéiques du lactosérum, en particulier les protéines du lactosérum dans les produits laitiers, sont liées à l'encrassement, avec l'effet couplé des paramètres du processus. Notre hypothèse est que le taux de cisaillement qui règne dans les évaporateurs pourrait être responsable de l'encrassement. Alors que plusieurs études ont examiné l'effet du cisaillement sur la dénaturation et l'agrégation des protéines de lactosérum, les découvertes contradictoires ne permettent pas de savoir ce qui se passe à la surface du matériau. Pour combler cette lacune, l'influence du cisaillement sur la dénaturation et l'agrégation des protéines de lactosérum a été étudiée à une température de dénaturation partielle fixe (65°C). Des solutions de protéines de lactosérum ont été préparées à une concentration de 5 % en poids et de 10 % en poids et ont été soumises individuellement à un traitement de cisaillement par rhéométrie - géométrie à plaques parallèles. Le traitement par cisaillement a été effectué à des taux de cisaillement variés allant

de 0s^{-1} à 200s^{-1} . La morphologie des agrégats a été étudiée pour ses caractéristiques qualitatives : distribution de taille, forme et structure, au microscope électronique à balayage, en fonction du taux de cisaillement et de la concentration en protéines. Les résultats ont révélé que l'augmentation du taux de cisaillement facilitait la croissance des agrégats à 5% en poids, alors qu'elle inhibait la croissance lorsque les taux de cisaillement étaient augmentés de 140 à 200s^{-1} à 10% en poids. Une augmentation du taux de cisaillement jusqu'à 200s^{-1} et de la concentration en protéines de 5% à 10% en poids de WPI a réduit la porosité des agrégats.

Mots clés : Concentration par vaporisation, Protéines de lactosérum, taux de cisaillement, Agrégat, Morphologie, dénaturation

Acknowledgments

The internship I had with UMR STLO (Unité Mixte de Recherche Science et Technologie du Lait et de l'Œuf), INRAE (Institut National de Recherche pour l'Agriculture, l'alimentation et l'Environnement), Institut Agro from 2 February 2023 to 31 July 2023 was a great chance for learning and developing professional skills. Therefore, it was a privilege and honor to be provided with the opportunity to be a part of one of the esteemed research units. I am also grateful for meeting so many wonderful people and professionals who led me through this internship period.

Notably, I would like to express my deepest gratitude and special thanks to the supervisor of the project Dr. LANOTTE Luca and to the co-supervisor Dr. LEE Jeehyun of STLO, who took time out to hear, guide and keep me on the correct path and allowing me to carry out this project, providing me with extremely valuable content both theoretically and practically.

I express my deepest thanks to Mr. JOANNY Loic and Mr. GOUTTEFANGEAS Francis of CMEBA (Centre de Microscopie Electronique à Balayage), University Rennes 1 for allowing me to use the facility to carry out my experimental work, as well as taking part in giving the necessary advice and technical experimental guidance.

It is my radiant sentiment to place on record my best regards and deepest sense of gratitude to Professor GALLAI Nicola of ENSFEA (École Nationale Supérieure de Formation de l'Enseignement Agricole) for his role in the coordination of this internship program in partial fulfillment to my MSc in Agro Food Chain Innovation and Sustainability.

I perceive this opportunity as a big milestone in my career development. I will strive to use gained skills and knowledge in the best possible way to attain my desired career objectives. I hope to continue cooperation with all of you in the future,

Sincerely,

MSIBI Zanele Pamela

Place: Rennes

Date: 10 July 2023

Contents

Abstract	I
Acknowledgments	III
List of Figures	VI
Chapter 1 Introduction	1
1.1 Background Information.....	1
1.2 Research hypothesis	1
1.3 Research objectives	2
Chapter 2 Literature Review	2
2.1 Dairy fouling in falling film evaporators.....	2
2.2 Different types of fouling deposits	3
2.3 Components of milk	3
2.4 Whey proteins.....	4
2.4.1 Whey protein denaturation and aggregation pathway.....	5
2.4.2 Parameters of whey protein denaturation and aggregation	6
2.4.3 Effect of shear in whey protein denaturation and aggregation.....	7
2.5 Methods/techniques for the analysis of the microstructure of whey protein aggregates	9
2.5.1 Background of scanning electron microscope	9
2.5.2 Basic components of a scanning electron microscope	10
2.5.3 Operation technique of a scanning electron microscope.....	10
2.6 Conclusion	11
Chapter 3 Materials and Methods	11
3.1 Experimental strategy	11
3.2 Preparation of whey protein stock solutions.....	12
3.3 Shear treatment	12
3.4 Whey protein aggregate characterization	15
3.4.1 Microstructure analysis by scanning electron microscope.....	15
3.4.2 Aggregate morphology observation protocol under scanning electron microscope	16
3.5 Whey protein aggregate elemental composition analysis.....	17
3.6 Data analysis	18
Chapter 4 Results and Discussion.....	18
4.1 Effect of shear rate on size and size distribution of whey protein aggregates.....	19
4.1.1 Effect on whey protein aggregates at $\leq 1\mu\text{m}$	19

4.1.2	Effect on whey protein aggregates at $\approx 10\mu\text{m}$	20
4.1.3	Effect on whey protein aggregates at $\geq 50\mu\text{m}$	22
4.2	Effect of shear rate on the shape and structure of whey protein aggregates.....	23
4.2.1	Effect on whey protein aggregates at $\leq 1\mu\text{m}$	23
4.2.2	Effect on whey protein aggregates at $\approx 10\mu\text{m}$	24
4.2.3	Effect on whey protein aggregates at $\geq 50\mu\text{m}$	26
4.3	Conclusion.....	27
Chapter 5	General conclusion and perspective.....	29
Bibliography	30

List of Figures

Figure 2. 1 Multiple effect evaporator.....	2
Figure 2. 2 An illustration showing the structure of β -lactoglobulin with its disulfide bonds (A) and bovine α -lactalbumin (B).....	4
Figure 2. 3 An illustration showing denaturation and aggregation of whey proteins	5
Figure 2. 4 A schematic presentation of a series of thermal-induced denaturation and aggregation.....	6
Figure 2. 5 Aggregated networks under a light microscope, from sheared samples of 10% <i>wt</i> whey protein isolate at a shear rate: (A) $78s^{-1}$ and (B) $126s^{-1}$, from $20^{\circ}C$ to $76^{\circ}C$	8
Figure 2. 6 Aggregated whey proteins under optical microscope from sheared samples of whey protein concentrations of (a) 5% <i>wt</i> , (b) 10% <i>wt</i> , (c) 20% <i>wt</i> , and (d) 30% <i>wt</i> , at $80^{\circ}C$..	9
Figure 2. 7 Operating principles of a scanning electron microscope equipped with energy-dispersive X-ray spectroscopy.....	10
Figure 3. 1 Global experimental protocol on the surficial aggregate characterization of unsheared and sheared whey protein isolate solutions.....	12
Figure 3. 2 Rheometer (Physica MCR 301 series: Anton Paar GmbH).....	13
Figure 3. 3 Sections of shear treatment protocol: preparation of whey protein solution on glass surface disc, initiation of shear treatment at 1mm gap, sample cover to limit evaporation.	13
Figure 3. 4 distribution of shear rates on the sample glass surface disc.....	14
Figure 3. 5 Photographs showing the visual appearance of sheared and non-sheared samples at 5% and 10% <i>wt</i> WPI upon fouling experimentation.....	15
Figure 3. 6 Metalization coating system (Leica EM ACE200) and Scanning Electron microscope (JOEL JSM - 7100F).....	16
Figure 3. 7 A schematic illustration showing whey protein aggregation observation and image capturing by scanning electron microscope..	17
Figure 3. 8 X-ray spectrometer monitor equipped with the scanning electron microscope showing quantified and identified whey protein chemical elements.	17
Figure 3. 9 A schematic representation of defined classes used to classify whey protein aggregates' shapes and structure.....	18
Figure 4. 1 Sections of 5% and 10% <i>wt</i> WPI without shear ($0s^{-1}$) and with shear ($0 - 200s^{-1}$), at $65^{\circ}C$ for 10 minutes. Images show aggregates at low magnification 5000x and high magnification 50000x, at approximately $1\mu m$	19
Figure 4. 2 A schematic illustration of whey protein β Lg onset denaturation and primary aggregation on surface material as a function of shear rate.	20
Figure 4. 3 Aggregate size distribution of sections of 5% and 10% <i>wt</i> WPI at a low magnification 1000x, at approximately $10\mu m$, sheared within rates $0 - 200s^{-1}$, at $65^{\circ}C$ for 10 minutes..	21
Figure 4. 4 A schematic illustration of whey protein β Lg onset secondary aggregation at $10\mu m$ as a function of shear rate.	21
Figure 4. 5 Aggregated WPI at low magnification of 1000x, approximately for 5% <i>wt</i> WPI and 250x, approximately $50\mu m$ for 10% <i>wt</i> WPI. Samples were sheared within $0 - 200s^{-1}$ at $65^{\circ}C$ for 10 minutes..	22
Figure 4. 6 A schematic illustration of hypothesized WPI aggregate propagation as a function of shear rate	23

Figure 4. 7 Aggregated 5% and 10% <i>w</i> t WPI at a high magnification of 50000x at 100nm scale. Samples were sheared within 0 - 200s ⁻¹ at 65°C for 10 minutes.....	24
Figure 4. 8 Data showing aggregate shape and structure frequency of occurrence for 5% and 10% <i>w</i> t WPI at ≈ 10μm, sheared at 0 - 200s ⁻¹ , at 65°C for 10 minutes..	25
Figure 4. 9 Aggregate shapes and structure of 5% and 10% <i>w</i> t WPI, at a high magnification of 10000x at an approximated 10μm size. Samples were sheared from 0 - 200s ⁻¹ , at 65°C for 10 minutes..	26
Figure 4. 10 Shape and structure of 5% and 10% <i>w</i> t WPI, taken at a high magnification of 10000x and 2500x for sizes 10μm and 50μm respectively. Samples were sheared within rate 0 - 200s ⁻¹ , at 65°C for 10 minutes..	27

Brief description of the research unit

The internship took place at the UMR STLO, one of the research units under INRAE and Institut Agro. The location of UMR STLO in the west of France coincides with the main production and processing sites for its two objects of study: milk, and eggs. These subjects are explored in the disciplinary areas of biochemistry, processing, and microbiology. The internship project was conducted in the team of PSF (Processing Structure and Functionality).



Chapter 1 Introduction

1.1 Background Information

Fouling is the build-up of unwanted deposits on the internal surfaces of manufacturing plants observed in food, textile, pulp and paper, chemical, petroleum, cement, glass, and primary metals industries (Garrett-Price et al., 1984). Certain unit operations such as separation and heat treatment are reported to be more prone to fouling than others (Fernandes et al., 2021). The layer of deposits formed during fouling leads to inefficient heat transfer which further translates into an increase in energy costs. The embedded fouling deposit layers may additionally provide a conducive site for thermophilic bacteria growth (Scott et al., 2007), negatively impacting the overall processed product specificities. The fouling phenomenon is extremely costly in additional ways: it limits the production throughout and overall product quality while escalating the high cost associated with the maintenance requirements of the damaged equipment, this in turn provides an environmental drawback (Bouman et al., 1988).

The dairy industry has received special attention owing to the high fouling rates (Wilson, 2018). Moreover, Gillham et al. (2000) state that “because milk and milk products in nature are thermosensitive, the vulnerability of fouling is high. The deposit constituents that have been indicated to play a huge role are proteins and minerals”.

Several studies evolve around understanding many probable product and process parameters that play a role in dairy fouling. However, there is narrow research work done on the detailed investigation of what occurs in the process flow at a microscopic scale. Thereby, the deposit mechanisms are still not well understood (Bansal & Chen, 2006). Different hypotheses have been investigated with attempts to find the links between protein denaturation and deposit formation on the surface material. Amongst these is the surface material which has been investigated for its probable role in fouling. Its properties, more particularly the surface roughness are thought to participate in the unfolding of whey proteins, leading to deposit formation (Piepiorka-Stepuk et al., 2016). Additionally, fouling has been hypothesized to also depend on temperature, the concentration of whey proteins, and shear rate (Wolz et al., 2016).

The study seeks to understand the impact of the shear rate on protein denaturation and aggregate formation at the solid-liquid interface. It can be interpreted as the sweeping effect of the product flow by gravity in the internal wall of evaporators (Mura & Gourdon, 2016). This study is in partial fulfillment of the ongoing project on Encrassement Thermique des Evaporation (ENTEVAP) between STLO and Unité Matériaux et transformations (UMET), a laboratory in Lille. The fouling mechanism in this project is studied based on microscopy, rheology, and microfluidics approaches. The scope of this study covers the microscopic branch of the project to provide a qualitative characterization of the morphological properties of whey protein deposits using a scanning electron microscope.

1.2 Research hypothesis

- The shear effect has an individual or combined effect with protein concentration and temperature in protein denaturation and aggregation (Fouling).

- Fouling depends on the interaction between, the concentration of whey proteins and the shear rate.

1.3 Research objectives

By applying conditions close to typical fouling during the evaporation process; the interest was to study the morphology of the aggregates formed on surface material (glass) using scanning electron microscopy, which is not possible to achieve with an optical microscope. The studied morphological variables were whey protein aggregate shape, structure, and size distribution.

Chapter 2 Literature Review

2.1 Dairy fouling in falling film evaporators

In falling film evaporators, thermo-sensitive milk-derived products are concentrated by evaporating a certain quantity of water constituting the product (Dunna & Srinivas Kishore, 2015). This processing step serves as an intermediate step for the production of dried milk-derived products (Rahaei *et al.*, 2019). The falling film evaporators are largely used in the dairy industry owing to their application of short residence time (between 10-20 min), low evaporation temperature (between 45 to 70 °C), and great heat transfer coefficient with low-temperature differences (Dehbani & Rahimi, 2018).

The most commonly used multi-effect installation in the dairy industries is shown in Figure 2.1. It is equipped with tunnels 1-2 mm thin that are separated, whose length can reach up to 18 m. To become even more energy efficient, the evaporator chambers are connected in series, and the generated water vapor is recycled in the series of operations. This results in reduced energy consumption (Approximately 1/n effect, n being the number of evaporators) (Zhang *et al.*, 2018).

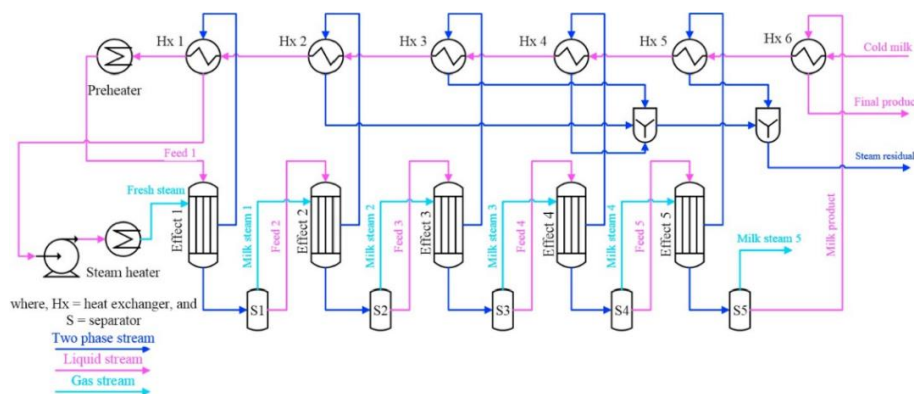


Figure 2. 1 Multiple effect evaporator. Reproduced from Zhang et al. (2018).

A distribution device distributes the product uniformly into the tubes of each evaporator tunnel by gravity. In brief, the three main parameters important during evaporation are time, temperature, and concentration. The concentration of the product increases from one tunnel to

the next and manufacturers pay close attention to this aspect due to the probable occurrence of fouling.

Each tunnel of a falling film evaporator is equipped with multiple tubes, and the product flows inside the tubes. A distribution device distributes the product uniformly in each tunnel by gravity, as the concentration increases from one tunnel to the next, manufacturers start to pay close attention. Dry patches inside the tubes could develop owing to the waves in product flow irregularities, vibration, or another source. The incomplete wetting of the tubes is due to mainly the lower mass flow rate of the product i.e., the unequal and unsteady liquid distribution at the top of the evaporation tubes causes the product to flow in rivulets at the edge of the dry patch. At this stage, the product either stops moving or moves very slowly. This further leads to the evaporator tubes becoming dry which causes significant fouling and may cause blocked tubes (Paramalingam *et al.*, 2000)

2.2 Different types of fouling deposits

Two kinds of most occurring fouling deposits have been identified in dairy industries. The initial one, known as Type A, is driven by whey protein deposits created between pasteurization temperatures (42 - 100 °C). Type A deposits are white, spongy, slightly dense and primarily constitute proteins (between 50% and 60%) specifically β -lactoglobulin (β Lg), minerals such as calcium phosphate (30% - 35%) as well as lipids (5%). The second fouling deposits are referred to as type B (also referred to as milk stones). They accumulate minerals that aggregate at higher temperatures *e.g.*, ≥ 105 °C. Type B deposits are generally hard, compact, granular in structure, grey, and dense. They consist primarily of about 70–80% minerals, dominantly calcium phosphate (70%). Additionally, type B deposits consist of proteins (15 - 20%) and lipids (4 - 8%) (Hagsten *et al.*, 2016). The main focus of the study is on the proteinaceous fouling deposit (type A) which has been linked to most cases of fouling.

2.3 Components of milk

Bovine milk is a complex biological fluid containing several components. It consists of 88% wt water in its continuous state with dry matter constituents that are either dissolved or suspended (Smirnova *et al.*, 2020). Formed in the solution is lactose with a percentage of 3.3% wt, and protein and mineral salts account for 3.2% wt and 0.7% wt, respectively. Both protein and a portion of the minerals exist in a colloidal suspension, while the rest of the minerals are formed in solution (Geurts, 2005). The proteins can be categorized into two groups: caseins and serum proteins which are produced after the precipitating of caseins (Fox, 2003). Caseins, the main milk proteins occupying about 80% of total proteins in milk include α S1, α S2, β , and κ -caseins (Pereira, 2014). The third group is the minor group of proteins which exists in the fat globule membrane and is less than 1%. Additionally, “milk proteins contain the nine essential amino acids required by humans, making it essential in the food industry” (Geurts, 2005).

2.4 Whey proteins

The second largest category of proteins - whey proteins are characterized by a clearly defined tertiary structure and are soluble in serum (Boland, 2011). Whey proteins are also referred to as the major nitrogen compounds remaining in milk after the precipitation of the caseins by acid (pH 4.6) or by rennet (pH \approx 6.7) (Silva *et al.*, 2013). They are heterogeneous and primarily comprise a particular class of globular proteins: including immunoglobulins (13%), bovine serum albumin (7%), α -lactalbumin (α Lac) (20%), β Lg (55%), minor proteins such as protease, lactoferrin and peptones (5%) (Boland, 2011). The total whey proteins represent around 20 % of the nitrogen in bovine milk (Jeurnink & Dekruif, 1995).

β Lg is a globular lipocalin protein with a molecular weight of \approx 18.4 kDa. It is the most bioavailable whey protein found in cow's milk (Kontopidis *et al.*, 2004). Moreover, it is characterized by an isoelectric point (pI) of roughly 5.4 (Indyk *et al.*, 2017); It additionally has a firm b-barrel core encompassed by one long and numerous short α -helices with two disulfides (SS) bonds which are “(Cys66–Cys160 close to the surface, Cys106–Cys119 in the core as well as one free cysteinyl thiol (SH) of Cys121 embedded in the core” that dictates the tertiary form of β Lg (Adams *et al.*, 2006). Alpha-lactalbumin (α La), the second most dominant whey protein consists of 123 amino acids and is identified by four disulfide bonds that include: all eight cysteines, alongside a calcium-binding site which guarantees that α -LA will fold correctly and have great molecular stability (Lam & Nickerson, 2015). α -LA is described as being acidic when present in its purest form and also monomeric and is made up of a molecular weight of 14 kDa (Lam & Nickerson, 2015).

“Due to the calcium bonds that are present at the asparagine residues, the protein - lactalbumin is more heat stable than other whey proteins” (De Wit, 1990). The various secondary structures of α Lac and β Lg are shown in Fig. 2.2. The secondary structure belonging to β Lg is made of 15% α -helix and 50% β -sheet, while that of α Lac is folded mainly as α -helix (47%) with approximately 6% β -sheet (Chandra *et al.*, 1998). According to Chandra *et al.* (1998), “the secondary structure of β Lg is composed of roughly 15% α -helix and 50% β -sheet, whereas that of α Lac is folded primarily as α -helix (47%) with only about 6% β -sheet”.

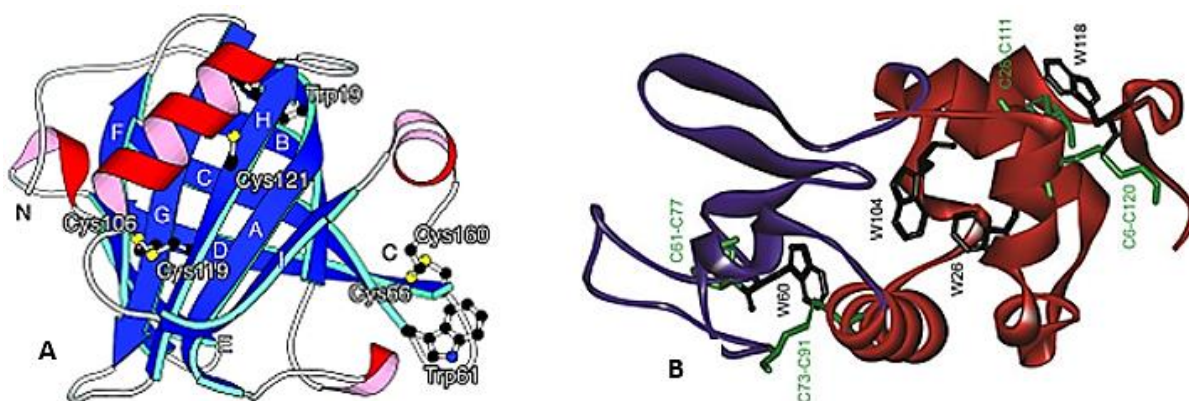


Figure 2. 2 An illustration showing the structure of β -lactoglobulin with its disulfide bonds (A) and bovine α -lactalbumin (B). Figures are reproduced from Yagi *et al.*, (2003) and Chrysinia *et al.*, (2000), respectively.

2.4.1 Why protein denaturation and aggregation pathway

The onset of aggregation that eventually adhere to surface material in evaporators occurs through partially folded protein intermediates, which are considered precursors to fully aggregated proteins. The deposition of aggregates in surface material is the result of several consecutive steps presented in Figure 2.3 **Step 1** - Conformation modification - this step is characterized by the conformation of the native structure (F) of the protein leading to the unfolded state (D), or other kinds of weak intermediates known as partially folded aggregates (R). These intermediates have exposed hydrophobic groups as a result of certain process parameters; they act as sticky or binding sites and are referred to as protein aggregation precursors.

Step 2 - Reversible Oligomerization also referred to as pre-nucleation. This step is characterized as the partial folding of intermediates oligomers through “the partial exposure of their hydrophobic groups to form reversible oligomers (Rx)”. These oligomers can be in a form of a dimer, trimer or tetramer, or even larger unit. This step is also referred to pre-nucleation step. **Step 3** - Nucleation. This step results in the formation of an irreversible oligomer (Ax), owing to an intermolecular beta-sheet structure that locks the oligomer together. **Step 4** - Condensation polymerization. This step is characterized by a further propagation of the aggregates, either through aggregate-aggregate coalescence mechanism (4a in Figure 2.3) or chain polymerization (4b in Figure 2.3) (Andrews & Roberts, 2007).

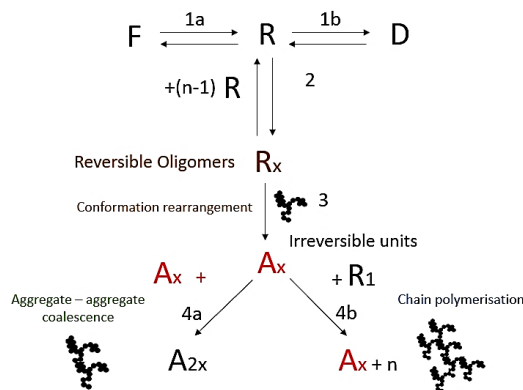


Figure 2. 3 An illustration showing denaturation and aggregation of whey proteins reproduced from Andrews & Roberts (2007). F stands for folded protein, D for unfolded protein, R for reactive monomer, Rx for reversible oligomer as well as Ax for smallest irreversible aggregate.

In falling film evaporators, the consequence is the formation of a base layer of the aggregates as fouling materials. These deposits adhere to the surface. The surface material has been indicated to facilitate deposit accumulation and stability through its reactions with active aggregates (Jebson *et al.*, 2009).

2.4.2 Parameters of whey protein denaturation and aggregation

Under certain process parameters, one of the main drawbacks that characterize whey proteins is their sensitivity to denaturation and fouling. “Since β -lactoglobulin is the primary constituent of whey proteins, it has been discovered that the degree of whey proteins denaturation is dependent on this element”, hence, its key role in the aggregation and fouling behavior of whey protein (De Wit, 1990).

2.4.2.1 Effect of temperature

The thermal effect has been studied intensively. De Wit (1990) indicated that, when exposed to temperatures around 70 °C, β Lg undergoes thermal denaturation. In brief, when milk is heated at temperatures over 70 °C, this, in turn, exposes their native β Lg protein ring containing reactive sulfhydryl groups. As a result, sulfur bridges begin to form between the β Lg molecules, and they further react with other forms of surrounding protein molecules to form aggregates. Figure 2.4 illustrates the intricate series of reactions leading to heat-induced denaturation and aggregation. In the physiological context of milk and whey protein, “a non-covalently I dimer stabilized by hydrogen bonds exists as β Lg at temperature 25 °C”. At this stage, a reversible dissociation of native dimers occurs as the first existing as the first form of heat-induced denatured β Lg with the increased temperatures up to and above 40 °C - dimers and monomers associate (de Wit, 2009). The native monomers change after additional heating - a reversible change referred to as ‘R-state’ which is characterized by minor modifications of the native protein status (Tanford *et al.*, 1959); As a result of the modifications, the thiol group that is conformed in the tertiary structure is liberated. Monomers are capable of forming aggregates in this state however at a low degree. The aggregation pronounces within the range \approx 65 °C – 70 °C; This condition results in the complete exposure of free thiol groups, marked on the molecule's external layer (Roefs & De Kruif, 1994). Additionally, the hydrophobic amino acids are made visible. Thus, their hydrophobic attraction to one another becomes stronger (Relkin, 1996). Also, any structural changes that are taking place are largely reversible.

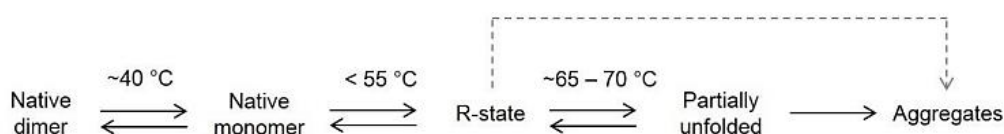


Figure 2. 4 A schematic presentation of a series of thermal-induced denaturation and aggregation. Reproduced from de Wit (2009).

According to Shimada & Cheftel (1988), above a temperature of \approx 130 °C, it has been established that the remaining protein structure unfolds, with a probable explanation for the chemical breakdown of disulfide bonds. On another note, it has been discovered that “at higher temperatures >100 °C, κ -caseins have been shown to react with the unfolding of β Lg and cause milk solution instability”. However, this reaction is very sensitive to pH changes (Connell & Fox, 2001). Other findings have shown that at higher temperatures > 120 °C, κ -caseins can dissociate from casein micelles and the micelles can aggregate through calcium phosphate bridges (Beliciu *et al.*, 2012).

2.4.2.2 Effect of pH

The link between the pH and the denaturation and aggregation of whey proteins has also been investigated. Covalent disulfide linkages have been reported to cause the aggregation of whey proteins at neutral or alkaline pH (Badii *et al.*, 2016). Mercadante *et al.* (2012) revealed that β Lg is sensitive when subjected to low pH. In agreement, Gulzar *et al.*, (2011) demonstrated that intermolecular disulfide linkages between aggregated proteins were more pronounced at pH 2.5.

2.4.2.3 Effect of mineral content

Pre-treatment before concentration by evaporation destabilizes the minerals in the milk solution. The precipitation of minerals from the milk due to the rise in concentration and temperature generates significant evaporator fouling, at higher temperatures they become less soluble. 'The most important minerals in milk are potassium, sodium, calcium, magnesium, chloride, and phosphate; dry weight mineral composition of minerals is about 5.4% by weight (Walstra *et al.*, 2005). It has long been acknowledged that the main component of mineral fouling from milk products is calcium phosphate. Research has widely covered the role that calcium phosphate plays in fouling of milk-derived products owing to the calcium ions concentration which is believed to assist in the unfolding and denaturing of proteins by creating cross-links between carboxyl groups and thus promoting conformational changes (Walstra *et al.*, 2005).

2.4.2.4 Effect of protein concentration

For the aggregation of whey proteins to occur, a minimum number of native proteins is needed, creating the first oligomers. The degree of association of the oligomers is dependent on protein concentration. High protein concentration is related to a higher degree of aggregation (Mehalebi *et al.*, 2008). Moreover, higher protein concentration conditions have been found to have a significant impact on the kinetics of denaturation. In agreement, Wolz *et al.* (2016) have also studied the parameter of protein concentration in whey protein denaturation and aggregation under the shear effect. When protein concentration was increased from 5% to 30% *wt* under shear and thermal effect, molecular collision increased causing an increased number of denaturation reactions and a higher rate of aggregation. The structure behavior also evolved from a more irregular porous at low concentration (5% *wt*) to a more compact and rounder form when protein concentration was increased above 5 *wt*%.

2.4.3 Effect of shear in whey protein denaturation and aggregation

Simmons *et al.* (2007) have proved that the shear effect indeed influenced the degree of whey protein denaturation and aggregation. In this scenario, native proteins unfolded (denaturation) as a result of collisions, which resulted in the formation of aggregates. The results from the study revealed that "aggregation was pronounced at higher temperatures (>75 °C) and

at higher shear rates ($\approx 625 \text{ s}^{-1}$) aggregates appeared to be denser and more rigid due to an increase in particle collisions which facilitates active agglomerates to interact directly with the evaporator surfaces". Walkenström *et al.* (1998) on the contrary, also studied the shear effect on whey proteins, with shear rates ranging from 0.5 and 126 s^{-1} , on 10% whey protein concentration. Whey protein solutions additionally were exposed to temperatures up to $82 \text{ }^\circ\text{C}$. Figure 2.5 shows the results that were obtained. Fractured aggregates were observed with the increase in shear rate. The shear rate was discovered to reduce aggregation, altering the microstructure of the aggregates to a reduced size as a function of the shear rate.

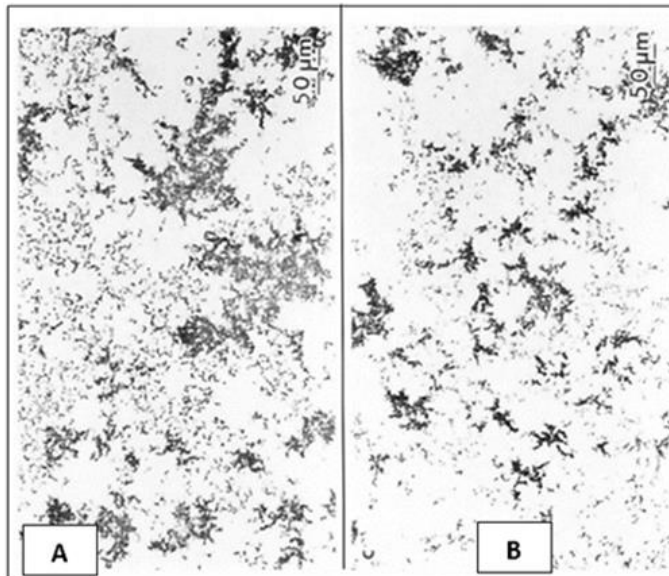


Figure 2. 5 Aggregated networks under a light microscope, from sheared samples of 10% *wt* whey protein isolate at a shear rate: (A) 78 s^{-1} and (B) 126 s^{-1} , from 20°C to 76°C . Reproduced from Walkenström *et al.* (1998).

The effect of shear rate with the coupled effect of protein concentration was studied by Wolz *et al.* (2016). Whey protein solutions at varied protein concentrations (5, 10, 20, and 30% *wt*) 80°C . In Figure 2.6, the results are displayed. The increases in whey protein concentration were found to hasten denaturation which is translated into the agglomeration appearance as a function of shear rate.

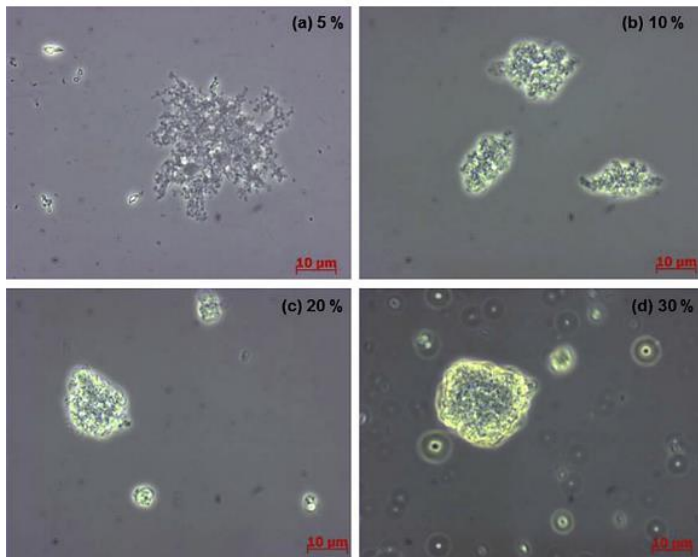


Figure 2. 6 Aggregated whey proteins under optical microscope from sheared samples of whey protein concentrations of (a) 5% *wt*, (b) 10% *wt*, (c) 20% *wt*, and (d) 30% *wt*, at 80°C. Reproduced from Wolz *et al.* (2016).

The detailed structure configuration of the aggregates with an increase in protein concentration tended to be compact, accompanied by a decrease in aggregate size with an increase in shear rate ($750 - 1452 \text{ s}^{-1}$). This result was explained to be attributed to the linear increase in shear stress as a function of protein concentration decrease. As a result, the shear stress limits aggregate growth. Conversely, at a low concentration (5% *wt*) with the function of shear rate results proved that the structure was more branched and porous. This was attributed to lower viscosity at lower protein concentrations, which further facilitates the adhesion of the particles. While various studies have examined the impact of shear on whey protein denaturation and aggregation, the majority of these studies have been conducted at high temperatures (above the denaturation temperatures of whey protein). Thereby, due to the probable confounding thermal effect, the specific effect of the shear rate is still not yet clearly understood. This study aims to fill in that gap by carefully investigating the effect of shear, using the temperature of 65°C which is below the denaturation of whey protein.

2.5 Methods/techniques for the analysis of the microstructure of whey protein aggregates

2.5.1 Background of scanning electron microscope

Instead of using light to create images, a scanning electron microscope (SEM) uses electrons (Abdullah & Mohammed, 2019). Thereby, it is considered one of the most comprehensive tools for examining and analyzing the morphologies of microstructures and is also used as a characterization tool of chemical compositions. It can use resolutions down to 0.2 nm. Electron microscopes can magnify their samples up to 100,000 of their original size (Zhou *et al.*, 2006).

2.5.2 Basic components of a scanning electron microscope

While the variations from model to model are seemingly endless, all SEMs share the same basic elements as shown in Figure 2.7.

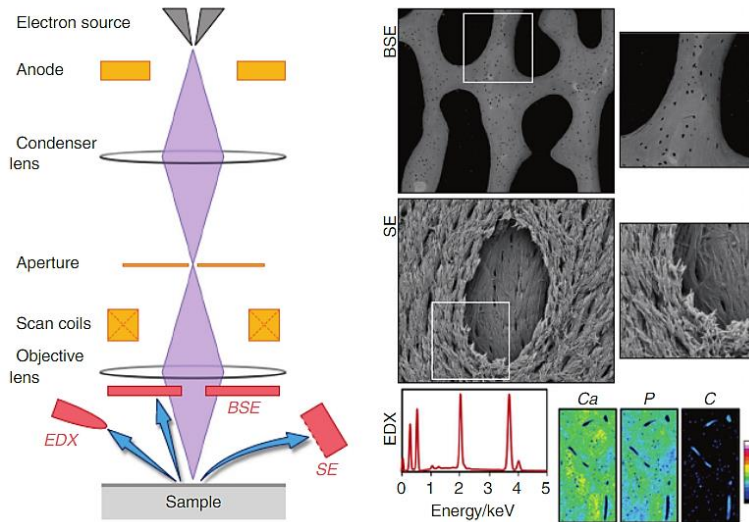


Figure 2. 7 Operating principles of a scanning electron microscope equipped with energy-dispersive X-ray spectroscopy. The basic parts of the scanning electron microscope are shown with the detected signals: backscattered electrons, secondary electrons, and energy-dispersive X-rays. Reproduced from Shah *et al.* (2019).

2.5.3 Operation technique of a scanning electron microscope

Inside the sample chamber of an SEM is where the specimen to be examined is placed after its metallization (coating) of thin conductive coatings (Figure 2.7). Different coatings are used that render the specimen conductive for observation. The most common coatings used include vaporized gold or palladium ions. The chamber is kept sturdy and insulated from vibration (vacuumed chamber), to avoid constant interference from air particles in the atmosphere that may distort the surface of the specimen. The process inside the SEM starts with the electron gun either placed at the top or on the bottom of the SEM. This gun generates a constant flow of electrons, which is necessary for the functioning of the SEM in imaging. The most common type used is the thermionic gun, which produces thermal energy to a filament (usually tungsten, which possesses a high melting point) to pull electrons away from the gun and toward the sample under test. Magnetic lenses bend the electrons' path and steer the electron beam to ensure the electrons go exactly where they're supposed to (Shah *et al.*, 2019).

When electrons come into contact with the specimen's coating, they cause the atoms on the sample surface to emit electrons. The detectors detect different signals upon the interaction of the electron beam with the specimen. They can be recorded by the secondary electrons detector which picks low-energy electrons, these are electrons propelled from the specimen's outer

surface. The surface topography of the object is most precisely pictured by secondary electrons. Other detectors such as backscattered electron detectors enable the pick-up of high-energy electrons, and they provide an in-depth specimen visualization. When an outer shell electron is displaced by an inner shell electron by an electron beam, X-ray detectors are used to detect the X-rays that are produced. “These detectors are typically used for element characterization using energy dispersive spectroscopy (EDS), as well as providing scientists with information about a substance's elementary composition” (Kannan, 2018).

2.6 Conclusion

The purpose of this state of art is to help the reader understand different aspects of dairy fouling posed in the evaporation process as a function of key milk components and process parameters. It can be concluded that whey protein particularly β Lg is susceptible to fouling. Also, the degree of denaturation and aggregation depends on whey protein concentration. Even though research is made on the shear effect on whey protein denaturation and aggregation, the shear effect has not been carefully established as it was largely observed at high temperatures above the denaturation of whey proteins, hence the need to establish more robust experimentations.

Chapter 3 Materials and Methods

3.1 Experimental strategy

The experimental strategy according to Figure 3.1 provides an overview of the pilot study experiment followed by a qualitative study. The morphology of whey protein aggregates was investigated.

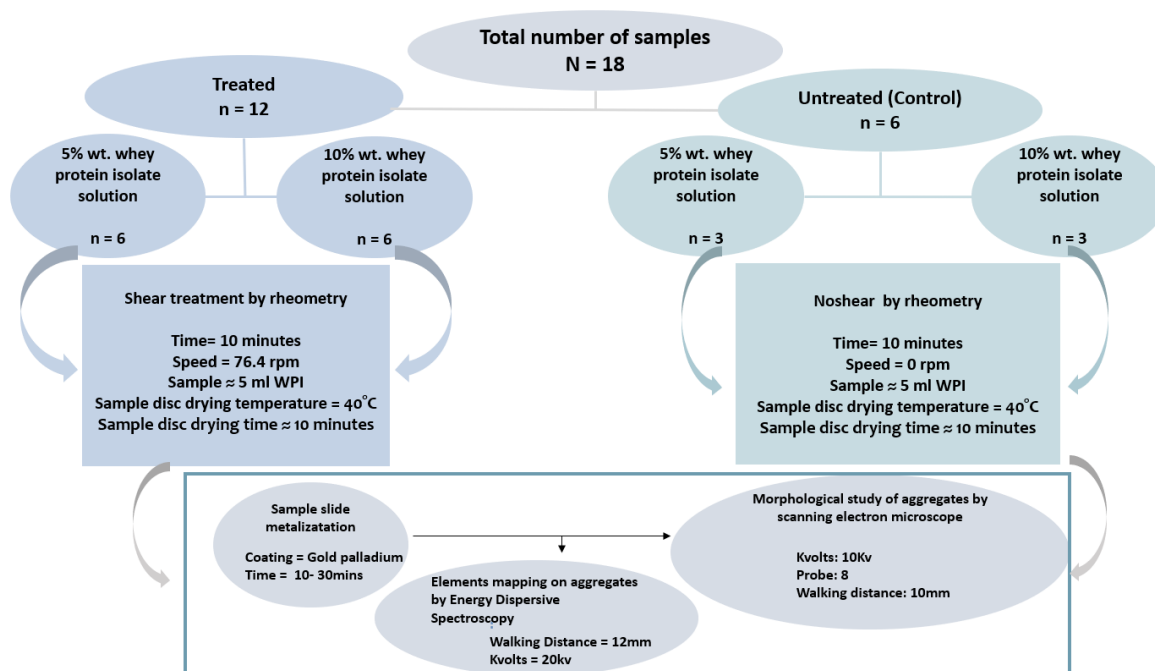


Figure 3. 1 Global experimental protocol on the surficial aggregate characterization of unsheared and sheared whey protein isolate solutions.

3.2 Preparation of whey protein stock solutions

Whey protein isolate (WPI) powder (FR 239 030 CE) was obtained from the Lactalis industry, in France. Its composition given by the supplier is composed of a dry protein of 92.6% wt and whey protein of 82.75% wt. The main whey protein components are α Lac and β Lg, which constitute respectively 20% and 50% of the total protein present.

The whey stock solution of 50 ml was made to 5% and 10% wt. by dispersing WPI powder in deionized water containing Sodium Azide (0.02 % wt) to prevent bacterial growth. Solutions were then stirred with a rotation velocity of 360 (rad/s), for about 24 h at ambient temperature (20 °C) until completely dispersed. The stock solution was then stored at 5 °C until usage at ambient temperature. The native pH of the whey protein (\approx 6.5) remained unadjusted.

3.3 Shear treatment

Whey protein aggregates were generated using shear treatment. A laboratory scale experimental process rheometer MCR 301 Anton Paar illustrated in Figure 3.2 was used. This rheometer is equipped with a parallel-plate geometry (PP25) to characterize surface anchored aggregates on the lower plate of this geometry with radius (R) = 2.5cm (Anton Paar GmbH, 2010).



Figure 3. 2 Rheometer (Physica MCR 301 series: Anton Paar GmbH).

Using a pipette, ~5mL of prepared whey protein solution was transferred to the sample glass disc adhered to the geometry plate using tape scotch, at an initial temperature of 40 °C (Figure 3.3 A). The geometry was then lowered and the sample temperature was left to equilibrate for 3 min before shear-heating profiles were undertaken (Figure 3.3 B). The fluid material was confined between the two plates with a gap of 1mm, with the upper plate moving at a constant speed (76.4 rpm) for sheared samples. The unsheared whey protein solutions at both 5% and 10% wt concentration were monitored under the same rheometry parameters with modification in the rotational speed, which was adjusted to 0rpm. Heating profiles start at 40°C and increased to the target temperature of 65°C. Within 10 minutes, the samples were sheared under steady shear between 0 to 200s⁻¹ before quiescent cooling to 40 °C upon shearing. In all experiments, a cover was placed over the system to minimize evaporation effects (Figure 3.3 C). Upon shear treatment, samples were removed from the geometry, and the whey protein excess solution was discarded. The sample glass discs were washed with ultrapure milli-Q water and then dried in an oven at 40°C for 10 min before being subjected to further analysis (as described in section 3.4).

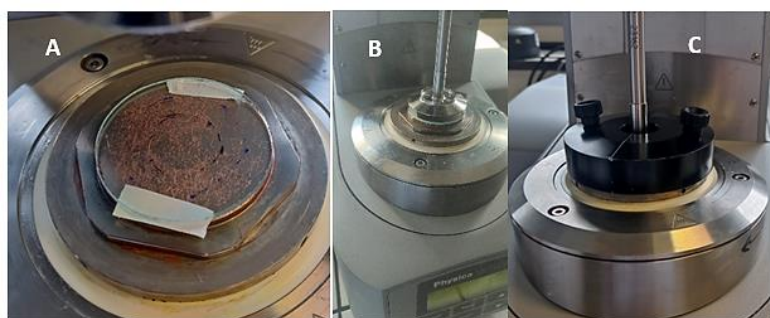


Figure 3. 3 Sections of shear treatment protocol: preparation of whey protein solution on glass surface disc (A), initiation of shear treatment at 1mm gap (B), sample cover to limit evaporation (C).

The spatial distribution of shear rates during shear was estimated on the regions of the sheared glass surface disc from the center. In the case of the parallel-plate geometry, both of

these kinematic quantities vary linearly with the radial coordinate r : shear rate ($\dot{\gamma}$) experienced by the fluid is given by the following calculations $\dot{\gamma} = \frac{\Omega \cdot r}{h}$... (1) which is related to the shear strain $\Upsilon = \frac{\theta \cdot r}{h}$... (2) (Barnes, 2000)

where: h is the gap between the plates, θ is the angular displacement, Ω is the angular Velocity. From the equation, shear strain (Υ) is related to the radius, r , gap height, h , and rotation angle θ . The change in strain rate (the speed or velocity at which deformation occurs) with time, at a given shear is kept at a constant radial distance at the defined zones of the sheared plate which is given by; $\dot{\gamma} = \frac{\Omega \cdot r}{h}$... (1) $\Omega = \frac{\dot{\gamma} \cdot h}{r} = \frac{200 \text{ s}^{-1} \cdot 0.1}{2.5} = 8 \text{ rad} \cdot \text{s}^{-1}$... (3)

The angular velocity for all the sheared regions on the glass disc surface was fixed based on the maximal outer edge of the sheared surface at 200 s^{-1} , alongside its measured radius of 2.5 cm. By using the equation (1), it is possible to estimate how the shear rate is distributed from defined zones of the sample disc i.e., periphery (P), intermediary (I), and center (C) (Figure 3.4).

Shear rates per zone

Shear rate_P = 140 – 200 s⁻¹

Shear rate_I = 80 – 140 s⁻¹

Shear rate_C = 0 – 80 s⁻¹

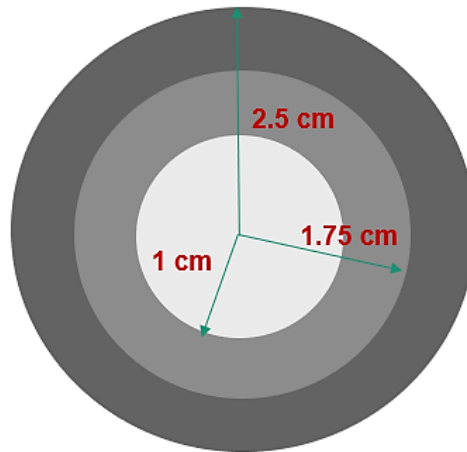


Figure 3. 4 distribution of shear rates on the sample glass surface disc.

The appearance of some examples of the sample sets upon fouling experiment is depicted in Figure 3.5, both without shear treatment - control (0 s^{-1}) and with shear treatment ($0-200 \text{ s}^{-1}$), at a steady temperature of 65°C for 10 minutes.

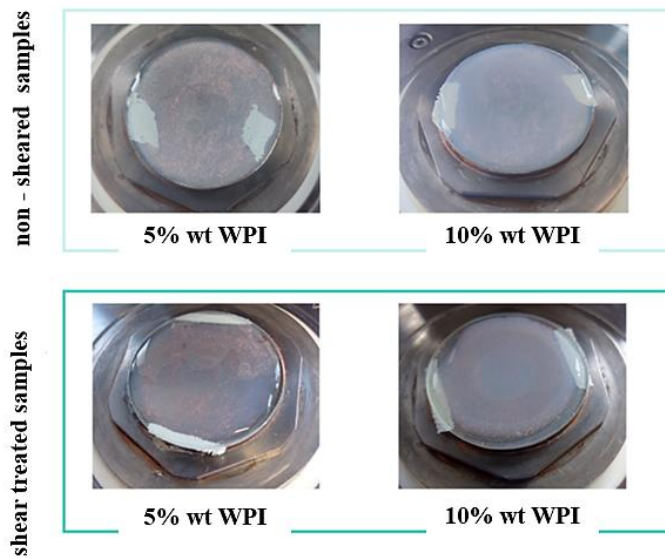


Figure 3. 5 Photographs showing the visual appearance of sheared and non-sheared samples at 5% and 10% *wt* WPI upon fouling experimentation.

3.4 Whey protein aggregate characterization

The morphology and chemical element of the whey protein aggregates were performed on a microscopic scale as a function of shear rate alongside the combined effect with protein concentration.

3.4.1 Microstructure analysis by scanning electron microscope

The dried sample glass disc which contained the whey protein aggregates was first sputter coated using the Leica EM ACE200 coating system (Figure 3.6 A) for ≈ 10 minutes (set time) in a vacuum-prepared chamber. A gold palladium conductive metal film was coated on the surface of the sample slide with a thin layer of about 10 nm. Upon coating, the samples were imaged by a field emission scanning electron microscope (JEOL JSM-7100F) presented in Figure 3.6 B, at an accelerating voltage of 10Kv, under a high vacuum and a working distance of 10mm. The topography of the whey protein aggregates was analyzed with the aid of a secondary electron detector at different scan sizes as outlined in section 3.4.2.

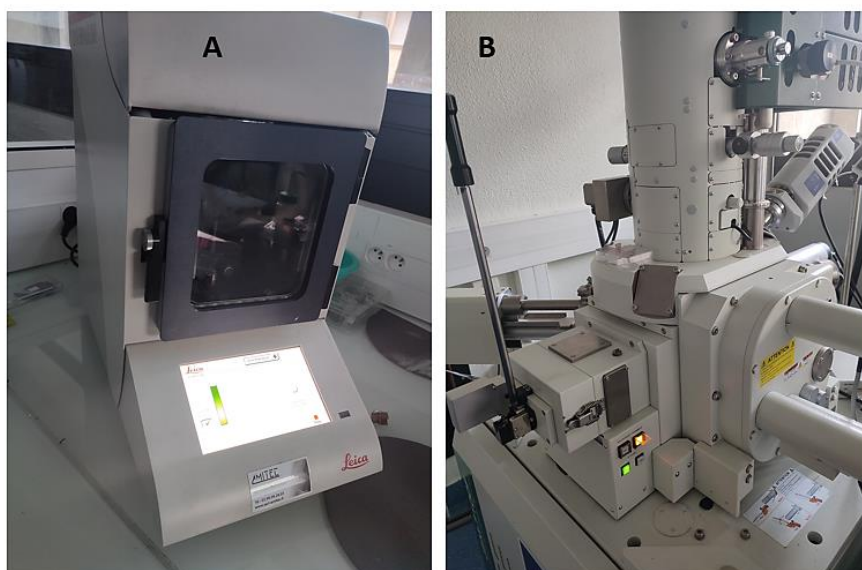


Figure 3. 6 Metalization coating system (Leica EM ACE200) shown in A and Scanning Electron microscope (JOEL JSM - 7100F) shown in B.

3.4.2 Aggregate morphology observation protocol under scanning electron microscope

Observation of whey protein aggregates was conducted according to the listed strategical objectives below. At each marked region on the glass surface disc shown in Figure 3.7, using a scanning electron microscope, one image was taken which contained the most aggregates at a low magnification to understand the aggregate size and size distribution. The second image on the very same region was taken for at least one of the aggregates at a rather higher magnification to understand the shape and structure of the whey protein aggregate. These characteristics variables were studied for aggregates sized $\leq 1 \mu\text{m}$, $\approx 10 \mu\text{m}$ as well as $\geq 50 \mu\text{m}$ at 5% and 10% *wt* WPI.

Observation objective 1: This observation was based on the hypothesized effect of shear rate, and the combined effect with protein concentration on protein unfolding, and in the formation of fouling initiating points on the surface material. The observation strategy was to focus on smaller aggregates sized $\leq 1 \mu\text{m}$ at magnifications: x5000 and x50000.

Observation objective 2: The second objective was based on the hypothesized effect of shear application and the combined effect with protein concentration: on the build-up of large aggregates at the size of $\approx 10 \mu\text{m}$ at a magnification of x1000 and zoomed magnification of x10000.

Observation objective 3: The third objective was based on the hypothesis of the propagation of aggregates on the surface material as a function of shear rate, and the combined effect with protein concentration. The observation strategy was to focus on typically much larger whey protein aggregates sized $\geq 50 \mu\text{m}$ at magnification x250, and a zoomed-in magnification of x10000 respectively.

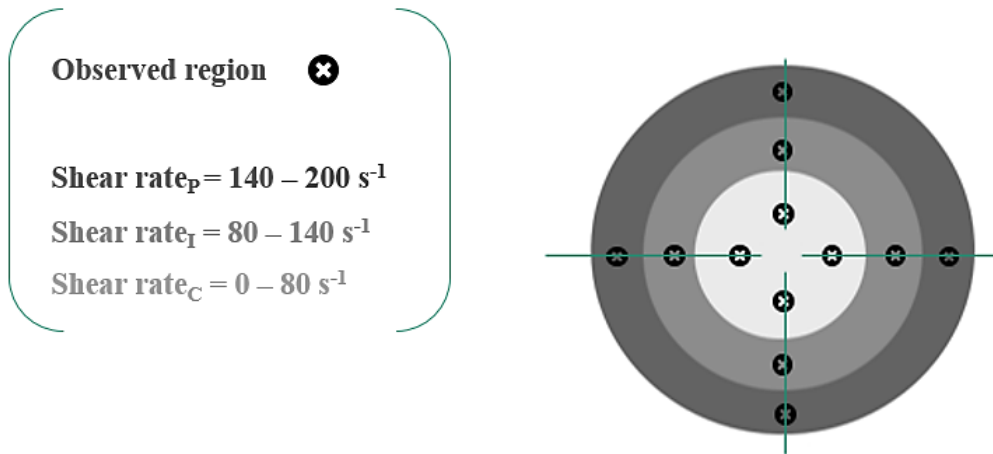


Figure 3. 7 A schematic illustration showing whey protein aggregation observation and image capturing by scanning electron microscope. The markings (x) represent the studied regions on the sample glass surface disc.

3.5 Whey protein aggregate elemental composition analysis

To control the aggregate selection process, the existence of the whey protein in the samples was examined with an energy-dispersive X-ray spectrometer equipped in the SEM. The element composition was studied with a special interest in sulfur and nitrogen which are characteristic features of whey proteins. This made it easy to select the aggregates of interest to the study. Imaging and elemental analyses were carried out in a vacuum chamber with an accelerating voltage of 20 kV, using AZTEC (Oxford Instruments) software for the EDS analysis. The position of the peaks in the spectrum identified the element, whereas the intensity of the signal corresponded to the concentration of the element (Figure 3.8). The element compositional information is picked down to the atomic level of the specimen.

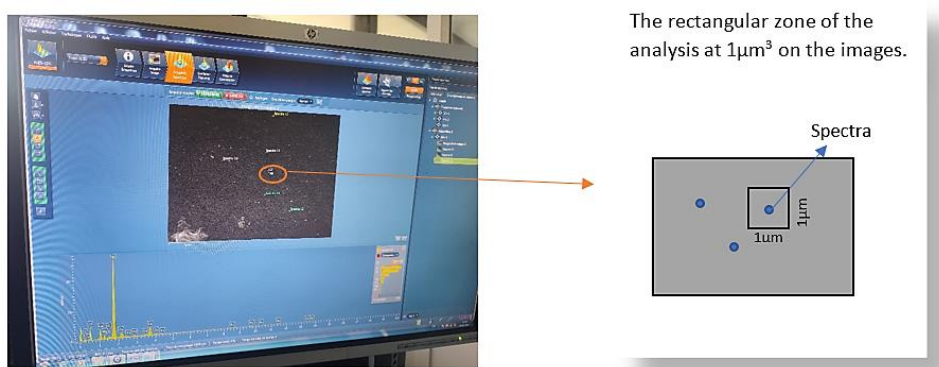


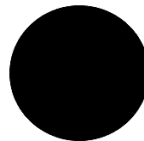
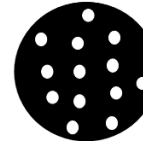
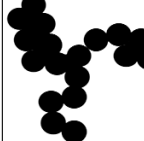
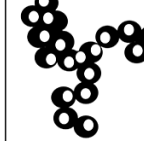


Figure 3. 8 X-ray spectrometer monitor equipped with the scanning electron microscope showing quantified and identified whey protein chemical elements.

3.6 Data analysis

After collecting the data, which was in the form of images, the images were studied before providing qualitative interpretation in light of the stated hypothesis. For the interpretation, three important qualitative variables of interest were aggregate size and size distribution. This entails qualitative information on how the observed whey protein aggregate under the scanning electron microscope is distributed on the surface as a function of shear rate. Aggregate shape and structure entail the study of details of the microstructure of the aggregate at a rather higher magnification under the scanning electron microscope as a function of shear rate and combined protein concentration effect. Heterogenous aggregates in the form of shape and structure were classified according to defined classes based on the frequency of occurrence per defined class using Excel. The data was interpreted through a graphical presentation.

Figure 3.9 schematically illustrates the different classes. It is worth noting that the classes were defined according to what was frequently observed under the scanning electron microscope.

Irregular		Globular		Branched	
Compact	Porous	Compact	Porous	Compact	Porous
					

Porous = with open pores

Compact = without pores (closed pores)

Figure 3. 9 A schematic representation of defined classes used to classify whey protein aggregates' shapes and structure. Dotted structures signify open pores while undotted structures.

Chapter 4 Results and Discussion

In this section of results and discussion, samples that were subjected to shear will be referred to as 'sheared samples. Unsheared WPI samples will be used as a reference to understand the effect of shear on aggregate morphological characteristics.

4.1 Effect of shear rate on size and size distribution of whey protein aggregates

4.1.1 Effect on whey protein aggregates at $\leq 1\mu\text{m}$

A section of the unsheared and sheared samples at 5% and 10% wt WPI is shown in Figure 4.1. At a lower magnification under no shear, the distribution of the aggregates appears to be roughly small in size ($<1\mu\text{m}$). Regardless of the protein concentrations, we can see the effect of shear, the aggregate appears to slightly increase at a size of size of $\geq 1\mu\text{m}$. With these results, we can confirm by saying the shear effect facilitates agglomeration or association. The aggregate size distribution takes a homogenous form without shear that is: aggregates maintain the same size and spread evenly. This even spreading is pronounced at low protein concentrations (5% wt WPI). When shear treatment is applied from 0 - 200s⁻¹ the spatial distribution of aggregates does not change while the aggregates variates. From intermediate shear rates 80 – 140s⁻¹ to maximal 140 – 200s⁻¹, the aggregates appear to become fewer at 10% wt WPI while at 5% wt WPI, we do not see much of a change within the same rates.

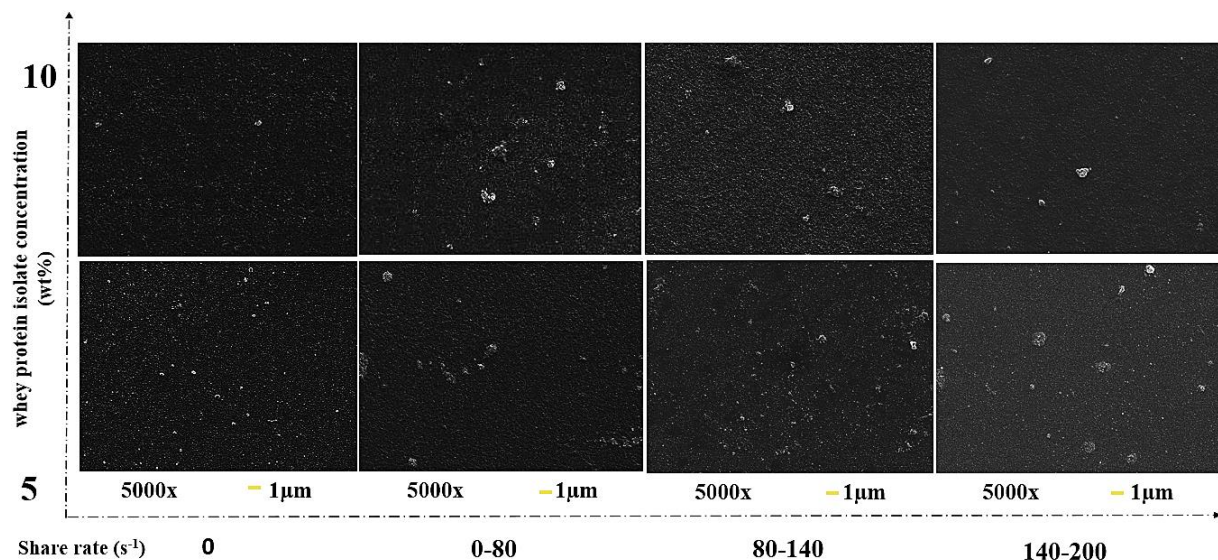


Figure 4. 1 Sections of 5% and 10% wt WPI without shear (0s⁻¹) and with shear (0 - 200s⁻¹), at 65°C for 10 minutes. Images show aggregates at low magnification 5000x and high magnification 50000x, at approximately 1 μm . Non-sheared WPI samples at 0 s⁻¹ are used as a reference.

These results can be transferred to what occurs in the falling film evaporators during evaporation. In brief, what eventually leads to surface fouling is characterized as a series of reactions that initiates from the whey protein unfolding. At slightly below whey protein denaturation temperature (65°C), whey proteins are already in a partially unfolded state. We have confirmed that shear rate can play a role in the degree of aggregation. We also saw the role of whey protein concentration in the influence of denaturation and aggregation, also indicated by Wolz *et al.*, (2016) in a similar study. The influence of the shear effect assists the partial temperature in the unfolding of whey proteins through particle collisions from the sheared field, in the surrounding fluid. This fully exposes the whey protein's thiol group. The

consequence is intermolecular disulfide bonding from the freed thiol group with surrounding whey protein molecules (Simmons *et al.*, 2007). At this stage, we see the appearance of the first reversible oligomers which we postulate to be primary aggregates at the size of $\approx 1\mu\text{m}$ as illustrated in Figure 4.2. Fouling deposition onto surface material during evaporation has been further explained that it consists of consecutive steps. These steps include Transportation: characterized by deposits being transferred to the surface material from the influence of shear flow. Adsorption: A base layer of fouling materials eventually adheres to the surface material. Build-up: The surface material's chemical reactions with the product can also participate in further accelerating the additional fouling material deposition (Jebson *et al.*, 2009).

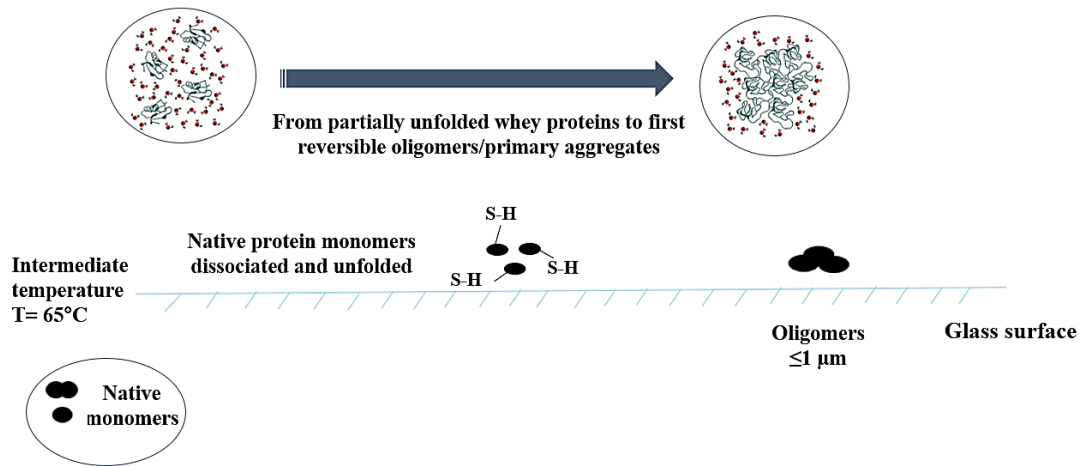


Figure 4. 2 A schematic illustration of whey protein βLg onset denaturation and primary aggregation on surface material as a function of shear rate.

4.1.2 Effect on whey protein aggregates at $\approx 10\mu\text{m}$

Figure 4.3 shows whey protein isolate aggregates distribution at $\approx 10\mu\text{m}$. when we observe aggregates at no shear condition (0s^{-1}), we see quite a few aggregates at $\approx 10\mu\text{m}$. Under a shear rate of between $0 - 80\text{s}^{-1}$ and $80 - 140\text{s}^{-1}$, extremely elongated aggregates start to form. The further increase of the shear rate to $140 - 200\text{s}^{-1}$ limits aggregate growth at high protein concentrations ($10\% \text{ wt}$) owing to the increased shear stress, while in low concentrations ($5\% \text{ wt}$) the aggregate size increases due to the increase in the number of collisions (Wolz *et al.*, 2016). As additionally explained by Vilotte (2021), in low and moderate shear rates the size ought to grow as the rate of collision does, increasing the size of monomers and oligomers. However, as the protein concentration increases, the size should decrease at higher shear rates since the aggregates might be damaged by shear forces. A conclusion can be drawn that the increase in protein concentration facilitates aggregate growth, while the increase in shear rate inhibits aggregate growth at high concentrations owing to the increased shear stress which correlates to shear rate increase. We can postulate that aggregate growth results from the rearrangement of first oligomers appearing at $\approx 1\mu\text{m}$ aggregates to form larger aggregates classified as secondary aggregates at the size of $\approx 10\mu\text{m}$, which is driven by the shear rate.

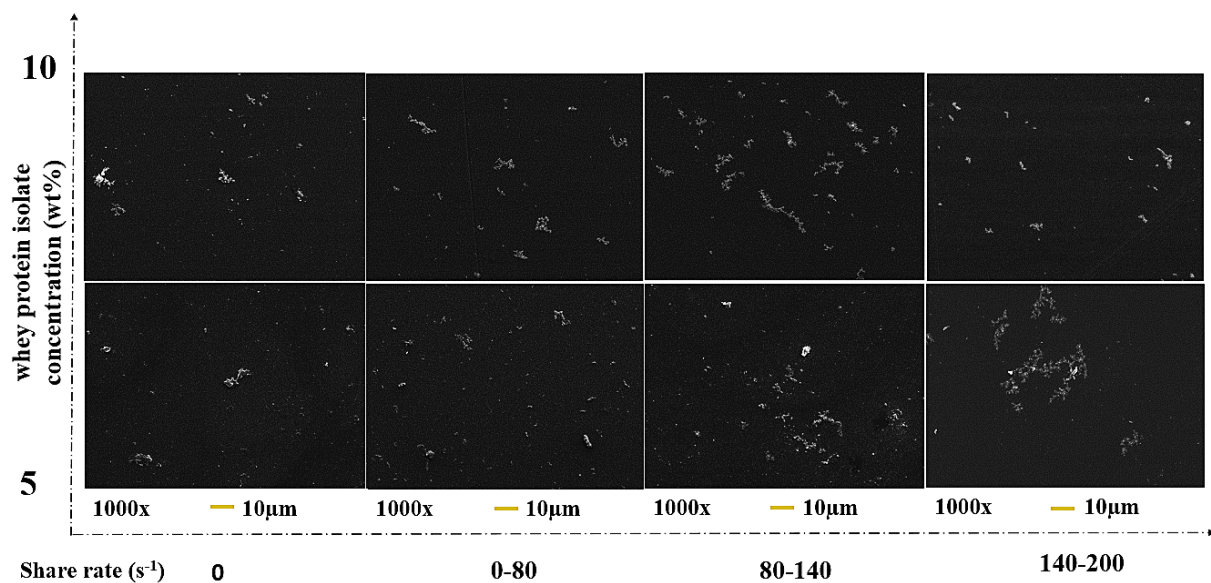


Figure 4. 3 Aggregate size distribution of sections of 5% and 10% *wt* WPI at a low magnification 1000x, at approximately 10µm, sheared within rates 0 - 200s⁻¹, at 65°C for 10 minutes. Non-sheared WPI samples at 0 s⁻¹ are used as a reference.

Figure 4.4 illustrates the hypothesized aggregate growth mechanism. The secondary aggregate growth mechanism has been disclosed to occur through aggregate-aggregate association (coalescence), also known as nucleation. Nucleation is characterized by the structural rearrangement of oligomers. This results in the formation of irreversible aggregates with higher molecular mass. The intermolecular beta-sheet structure has been reported to provide points of association that lock the aggregates together, forming activated βLg intermediates (Lefèvre & Subirade, 2000). With the influence of shear rate accompanied by protein concentration, the entire denaturation reaction quickens (Tolkach & Kulozik, 2007).

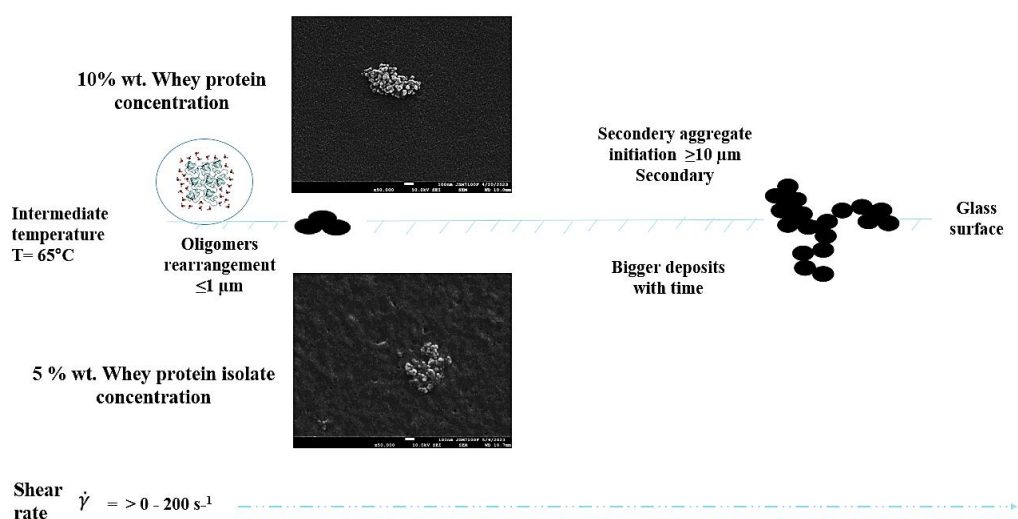


Figure 4. 4 A schematic illustration of whey protein βLg onset secondary aggregation at 10µm as a function of shear rate.

4.1.3 Effect on whey protein aggregates at $\geq 50\mu\text{m}$

What was worth noting was the polymerized formed larger aggregates at $\geq 50\mu\text{m}$. Surprisingly, these aggregates were only observed when the protein concentration was increased to 10% *wt* WPI under only shear conditions. Under the scanning electron microscope, these aggregates were branched with the resemblance of networks. Results presented in Figure 4.5 indicate the size distribution of the aggregates when both concentrations of 5% and 10% *wt* WPI were compared. As the protein concentration increases from 5% *wt* to 10% *wt* WPI, so does the size of the aggregate. Although the aggregates at 10% *wt* WPI under a higher shear rate (140 - 200s⁻¹) seem to be bigger than in a low concentration under the same shear condition, their growth seems to be halted as previously explained. Also, at this phase, the irregularity of aggregate size dispersion is observed as a function of the shear rate. We get more varied-sized aggregates at the intermediate shear region 80 - 140s⁻¹. The polymerization effect is postulated to result from largely the association of active secondary aggregates (Andrews & Roberts, 2007). The influence of shear leads to subsequent secondary aggregate interaction, and subunits are added to the growing aggregates, a process referred to as 'chain polymerization' (Dunstan et al., 2009).

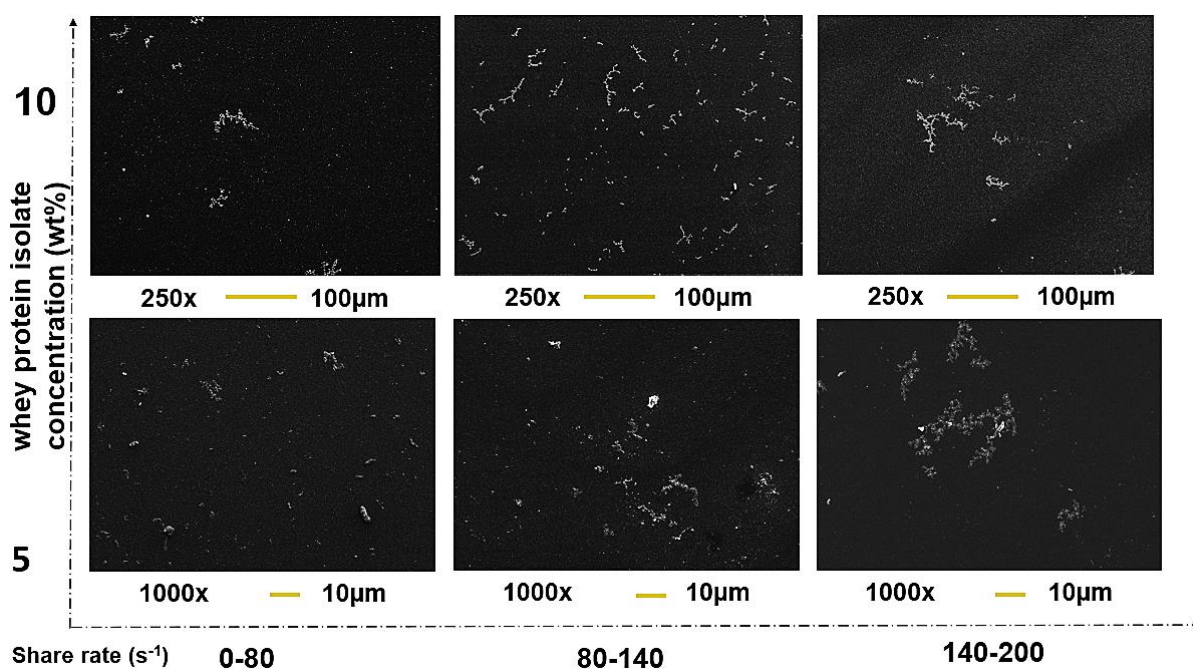


Figure 4. 5 Aggregated WPI at low magnification of 1000x, approximately for 5% *wt* WPI and 250x, approximately 50µm for 10% *wt* WPI. Samples were sheared within 0 - 200s⁻¹ at 65°C for 10 minutes. Non-sheared WPI samples at 0s⁻¹ are used as a reference.

Based on Figure 4.6, a summary of hypothesized aggregate propagation is outlined. It can be postulated that aggregate propagation occurs through the formation of an intermolecular disulfide bond between already exposed S-H bonds of an activated βLg aggregate. As a result, polymerization is induced arising from intermediate secondary aggregates. In response to

repeated aggregation, facilitated by increased denaturation from increased protein molecules, the result is multiple interlinking occurrences characterized by aggregate-aggregate propagated network structures. The termination of the aggregation reaction is signaled by the absence of a reactive S-H group (de Wit, 2009). A similar discussion has also been reported by Dunstan *et al.* (2009); the reported postulation was that the formation of the observed whey protein fibrils is attributed to β Lg that has been unfolded. Hence, β Lg produces oligomeric nuclei during the shear exposure of the whey protein solutions. The aggregate association that occurred eventually resulted in the formation of fibrils' nuclei at the shear rate of 150s^{-1} . The results showed a major acceleration in fibril development, which is not significantly different from our findings at the intermediate shear rate within $80 - 140\text{s}^{-1}$.

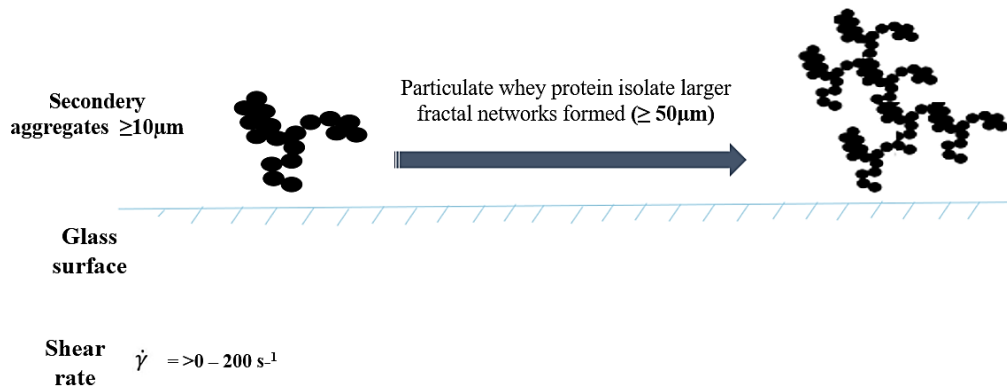


Figure 4. 6 A schematic illustration of hypothesized WPI aggregate propagation as a function of shear rate

4.2 Effect of shear rate on the shape and structure of whey protein aggregates

4.2.1 Effect on whey protein aggregates at $\leq 1\mu\text{m}$

Due to the complication of the aggregate size at $\approx 1\mu\text{m}$, the state of aggregation did not show much of a difference in terms of shape and structure. As a result, it was complicated to classify the structures. Images presented in Figure 4.7 at higher magnification however provides an approximated summary of the aggregate shape and structure details, observed at $\leq 1\mu\text{m}$. Under no shear and shear effect, and regardless of the protein concentrations, there is no difference in the structure of aggregates. Aggregates are observed to be porous and globular with slight irregularity. This indifference of aggregate porosity of the unsheared WPI samples at 0s^{-1} was also observed by Walkenström *et al.* (1998), whereby results indicated that aggregates were composed of pores. The aggregation under no shear is postulated to be from the effect of the intermediate heat, allowing the partial unfolding of the whey proteins. Additionally, under no shear effect, the aggregates slightly increase with the increase in protein concentration while maintaining porosity regardless of the WPI concentration. On the contrary, under the shear condition, compactness is suggested with an increase in shear rate regardless of the protein concentration. However, at $10\% \text{ wt}$ WPI and low shear rate ($0 - 80\text{s}^{-1}$), the degree of compactness is more pronounced while at $5\% \text{ wt}$ WPI at the same shear rate porosity is more pronounced. Similar observations were reported by Wolz *et al.* (2016) on shear-induced

aggregates at a varied shear rate of 100 s^{-1} to 1452 s^{-1} , for 5% and 10% *wt* WPI. Under low shear rate conditions at a low protein concentration of 5% *wt* WPI, this observation was explained by the low protein concentration from the surrounding fluid during shear treatment. The coupled effect of a low shear rate is enough to allow the particles to slightly stick to each other with the influence of the low fluid flow from the sheared field. As a result, aggregates appear to be in an arrangement of flat strings. This however is not the case at high protein concentrations (10% *wt* WPI) regardless of the shear rate condition, where aggregates appear to be packed in an agglomerated manner, owing to the increased number of protein molecules that influences the association at a higher impact from the numerous particle collision.

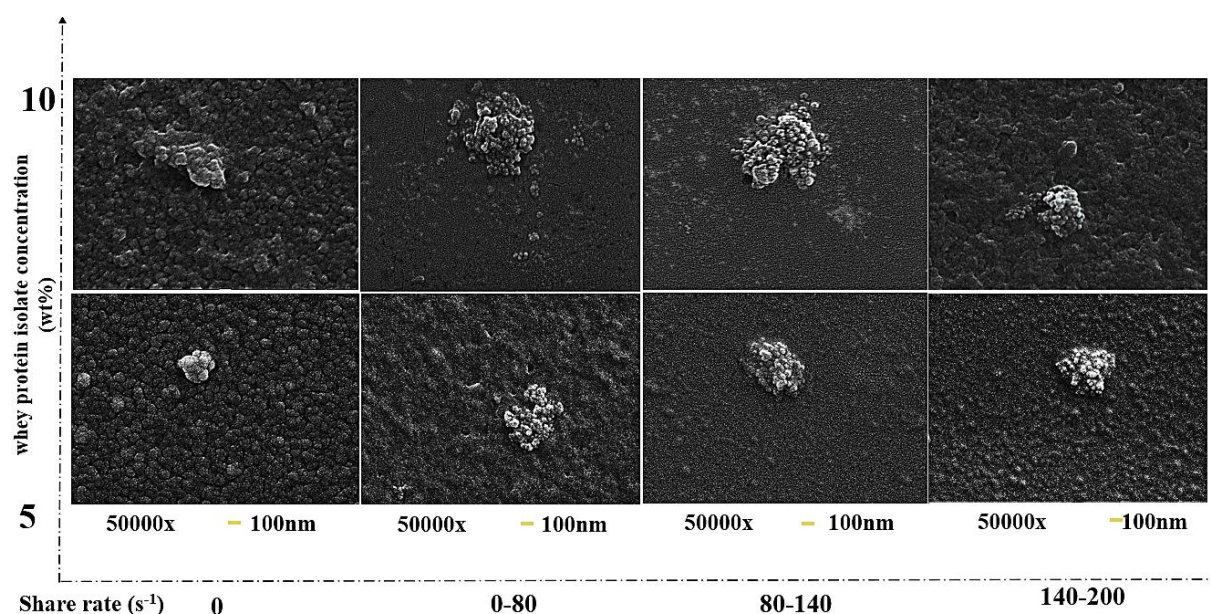


Figure 4. 7 Aggregated 5% and 10% *wt* WPI at a high magnification of 50000x at 100nm scale. Samples were sheared within 0 - 200 s^{-1} at 65°C for 10 minutes. Non-sheared WPI samples at 0 s^{-1} are used as a reference.

4.2.2 Effect on whey protein aggregates at $\approx 10\mu\text{m}$

When individual aggregates of $\approx 10\mu\text{m}$ size were observed at higher magnification, a variety of shapes and structures was observed. Hence, the aggregates were put into classes to further understand the frequency of occurrences of varied shapes and structures under the defined classes. The data presented in Figure 4.8 highlights the result of classification and frequency of occurrence of each class of shape and structure. The data is based on a basis of 20 aggregates as 100%, and the figure shows data obtained for 5% and 10% *wt* WPI at different shear rates. We observe that 100% of the aggregates are irregular porous under no shear condition at 5% *wt* WPI. At this concentration under shear conditions, the porous shape is predominant over the compact shape. The more shear rate is applied the more the branched porous formed aggregates become a majority than the irregular shape. At 10% *wt* WPI on the other hand, we see the exact opposite, the level of compactness is more prominent than the level of porosity. Even though

we observe a high number of branched porous aggregates than in 5% *wt* WPI, these branched aggregates become rare as a function of shear rate. Also, we observe more compact irregular shapes than porous irregular shapes. This is in accord with the suggested hypothesis of whey protein aggregation dependency on the degree of protein concentration.

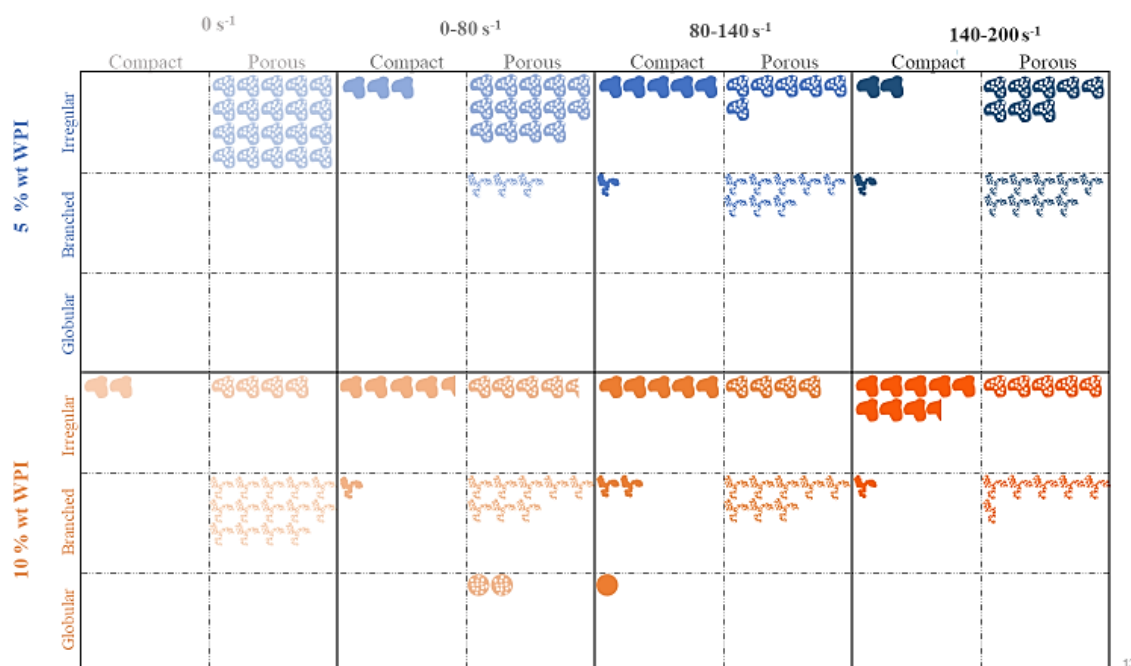


Figure 4. 8 Data showing aggregate shape and structure frequency of occurrence for 5 and 10% *wt* WPI at $\approx 10\mu\text{m}$, sheared at 0 - 200s⁻¹, at 65°C for 10 minutes. Non-sheared WPI samples at 0 s⁻¹ are used as a reference.

Taking a closer look at the individual aggregates, Figure 4.9 summarises the coupled effect of protein concentration and shear rate when comparing concentrations of 5% and 10% *wt* WPI, under the scanning electron microscope. Under no shear condition (0s⁻¹), aggregates seem to be loose and highly porous and soft textured, we start getting defined structures with shear effect. A decrease in porosity is suggested with an increase in both shear rate and protein concentration. These results are in accord with findings from Dunstan *et al.* (2009) where βLg was studied under shear flow rate 150s⁻¹ at 10% *wt* WPI in bulk solution. At 5% *wt* WPI, we tend to get more branched porous shapes as a function of shear rate, while at 10% *wt* WPI we get the inverse: porous branched form appears from a low shear rate 0- 80s⁻¹ up to the intermediate shear rate 80 - 140s⁻¹. At a maximal shear rate of 140 - 200s⁻¹, aggregates appear to be more irregular than branched.

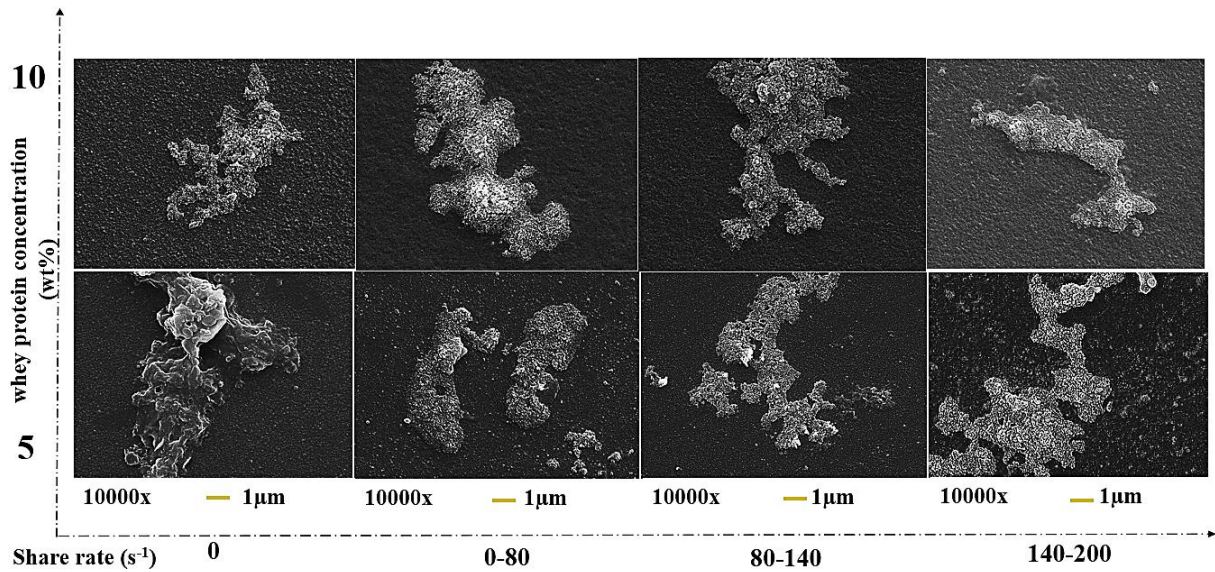


Figure 4. 9 Aggregate shapes and structure of 5% and 10% *wt* WPI, at a high magnification of 10000x at an approximated 10 μ m size. Samples were sheared from 0 - 200s⁻¹, at 65°C for 10 minutes. Non-sheared WPI samples at 0 s⁻¹ are used as a reference.

4.2.3 Effect on whey protein aggregates at $\geq 50\mu$ m

Figure 4.10 shows single aggregates when compared to 5% and 10% *wt* WPI. It is worth noting that aggregates at $\geq 50\mu$ m were only observed at 10% *wt* WPI sheared condition. All aggregates were branched and hence were classified under the branched compact class. The details of the branches as a function of shear rate appear to be rather different. At low shear rates regardless of the protein concentration, the aggregates are denser. The low shear rate condition is also characterized by the low fluid flow of the surrounding fluid during shear treatment. This particular shear rate provides time for particles to stick together forming dense regions as indicated by the thick branches. However, the aggregates tended to become thinner and branched with a shear rate increase. Additionally, these branches seem to become weak. This is in agreement with Dunstan *et al.* (2009) whereupon shear treatment (0 - 150s⁻¹) was applied to whey protein solutions. “Two types of fibrils were observed as a function of shear rate: thick (5–8 nm) fibrils and thin (~2 nm) fibrils” even though aggregation was studied in a bulk state. In other similar findings, Moakes *et al.* (2015) studied the effects of shear and thermal history on whey protein suspensions at 10% *wt* WPI, where shear rates were up to 800 s⁻¹. Results revealed that at a low shear rate, discrete dense aggregates (>120 μ m) were obtained which tended to decrease (<40 μ m) at higher shear rates. This result is confirmed by the fracturing of the networks mainly observed at high concentrations with an increase in shear rate, more announced in the higher shear rate (140 - 200 s⁻¹) from the increased shear forces.

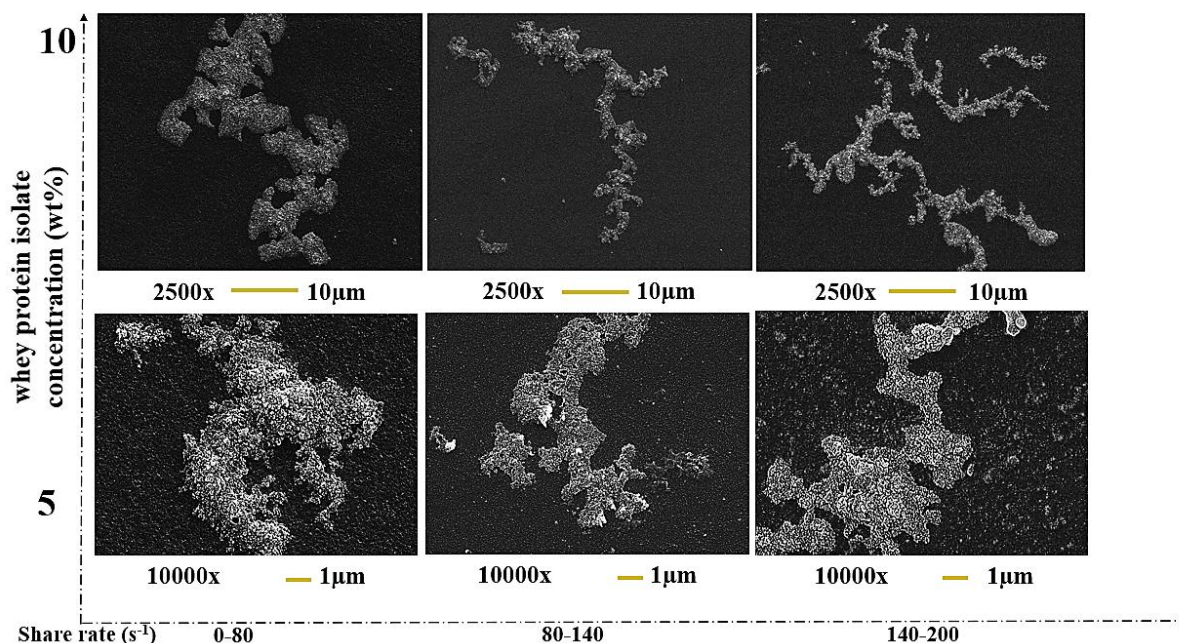


Figure 4.10 Shape and structure of 5 and 10% wt WPI, taken at a high magnification of 10000x and 2500x for sizes 10µm and 50µm respectively. Samples were sheared within rate 0 - 200s⁻¹, at 65°C for 10 minutes. Non-sheared WPI samples at 0s⁻¹ are used as a reference.

The fracturing phenomenon at a high shear rate has also been reported by Walkenström *et al.* (1998) on 10% wt WPI subjected to shear effect. In this study, we postulate that these aggregates would reduce in size and singulate if the shear rate were further increased at high concentrations. This has already been observed by Vilotte (2021) who studied shear-induced whey protein solutions. Indications highlighted that with the incremental shear rate from 53s⁻¹ to 2666s⁻¹, there was a breakdown of aggregates and growth was limited. This was explained by the less encounter time which reduced aggregation. Thereby, particles were reported to remain individual at the highest shear rates.

4.3 Conclusion

In this section, scanning electron microscopy allowed us to study and characterize whey protein aggregates in terms of size distribution, shape, and structure. In the first section, we studied the impact of shear established by rheometry- parallel plate geometry. We observed the impact of shear with the coupled effect with protein concentration in the postulation of whey protein denaturation and aggregation of whey proteins, dominantly βLg. First, we looked into the development of the first oligomers (postulated as primary aggregates). In the second part, we wanted to understand how these small aggregates at 1µm can lead to the development of aggregate accumulation at ≈10µm (intermediate aggregation). In the last part, we wanted to understand the onset of aggregate polymerization stemming from adhered aggregates on the surface's material. The results and discussion presented shed light that whey protein aggregate

morphology (size distribution, shape, and structure) can be impacted by shear rate as well as the degree of protein concentration.

Chapter 5 General conclusion and perspective

During this master's internship, a pilot study experimentation under conditions close to process conditions inside a falling film evaporator helped us understand the fouling phenomenon. The morphological characteristics (whey protein aggregate size distribution, shape, and structure) of whey protein aggregates were studied due to the denaturation and aggregation. Whey protein isolate solutions adjusted for 5% and 10% *wt* were subjected under carefully controlled evaporation conditions: shear rate that varied from 0-200s⁻¹ with a fixed temperature below the denaturation temperature of beta-lactoglobulin (65°C). In this study, we observed the impact of the shear effect with the coupled effect of whey protein concentration on whey protein aggregate morphology resulting from denaturation and aggregation. At temperatures below the denaturation point, whey protein aggregates are already partially unfolded, we have seen the additional effect of shear in assisting the whey protein in their unfolding through particle collisions. The study of whey protein aggregates by scanning electron microscopy showed different morphological characteristics as a function of shear rate and protein concentration.

A conclusion can be drawn that shear rate influences aggregation for the first oligomers ($\leq 1 \mu\text{m}$). We do not observe much of a difference between the aggregate structures which were observed to be globular porous with a slight irregularity. However, porosity was more pronounced for sheared 5% *wt* WPI aggregates at a low shear rate (0-80s⁻¹). For aggregates sized $\approx 10\mu\text{m}$ regardless of the concentration, porosity was reduced with the increase in shear rate. At 5% *wt* WPI, an increase in shear rate influenced aggregate growth. Additionally, aggregates became more branched than irregular, while they became more irregular than branched at 10% *wt* WPI. Also, at 10% *wt* WPI, aggregation was observed from a low shear rate of 0 - 80s⁻¹ to an intermediate shear rate of 80 - 140s⁻¹. Regarding aggregates observed at $\geq 50\mu\text{m}$, an increase in protein concentration up to 10% *wt* WPI resulted in the formation of big aggregates, evidently seen on the surface of the shearing plate of the parallel geometry during experimentation. At high magnification, aggregate density was more pronounced at shear rates between 0 - 80s⁻¹, while with the increase in shear rate, aggregates became less dense. They became thinner to the point of fracturing at a maximal shear rate of 140 - 200 s⁻¹.

The study provides the basis of knowledge not only for the dairy industry but other industries that face fouling challenges in process operations. The results can be used in estimating and manipulating different process parameters such as product composition, temperature, and shear rate in falling film evaporators. One of the perspectives could be: rather than using glass surfaces we can use stainless steel used in real-life evaporators. It would have been interesting also to try cone plate geometry under varied shear rates, as well at other varied concentrations such as in 15%. However, time was a limiting factor in fulfilling all the desired experimental variables. It remains a challenge for research coherence in fully understanding the aspects of fouling and while this phenomenon cannot be fully eradicated, its reduction remains possible. Therefore, more string of studies on dairy fouling, with a focus on falling film evaporators (commonly used evaporator type in the dairy industry) is required to gain a better understanding underlying the concepts of fouling to build robust predictive coherent results for reference.

Bibliography

- Abdullah, A., & Mohammed, A. (2019, janvier 5). *Scanning Electron Microscopy (SEM): A Review*. 2018 International Conference on Hydraulics and Pneumatics - HERVEX, Băile Govora, Romania.
- Adams, J. J., Anderson, B. F., Norris, G. E., Creamer, L. K., & Jameson, G. B. (2006). Structure of bovine β -lactoglobulin (variant A) at very low ionic strength. *Journal of Structural Biology*, 154(3), 246-254. <https://doi.org/10.1016/j.jsb.2005.12.010>
- Andrews, J. M., & Roberts, C. J. (2007). A Lumry–Eyring Nucleated Polymerization Model of Protein Aggregation Kinetics: 1. Aggregation with Pre-Equilibrated Unfolding. *The Journal of Physical Chemistry B*, 111(27), 7897-7913. <https://doi.org/10.1021/jp070212j>
- Anton Paar GmbH. (2010). *Basics of rheology: Anton Paar Wiki*. Anton Paar. <https://wiki.anton-paar.com/en/basics-of-rheology/>
- Badii, F., Atri, H., & Dunstan, D. E. (2016). The effect of shear on the rheology and structure of heat-induced whey protein gels. *International Journal of Food Science & Technology*, 51(7), 1570-1577. <https://doi.org/10.1111/ijfs.13126>
- Bansal, B., & Chen, X. D. (2006). A critical review of milk fouling in heat exchangers. *Comprehensive Reviews in Food Science and Food Safety*, 5(2), 27-33. <https://doi.org/10.1111/j.1541-4337.2006.tb00080.x>
- Barnes, H. A. (2000). Measuring the viscosity of large-particle (and flocculated) suspensions—A note on the necessary gap size of rotational viscometers. *Journal of Non-Newtonian Fluid Mechanics*, 94(2-3), 213-217. [https://doi.org/10.1016/S0377-0257\(00\)00162-2](https://doi.org/10.1016/S0377-0257(00)00162-2)
- Beliciu, C. M., Sauer, A., & Moraru, C. I. (2012). The effect of commercial sterilization regimens on micellar casein concentrates. *Journal of Dairy Science*, 95(10), 5510-5526. <https://doi.org/10.3168/jds.2011-4875>
- Boland, M. (2011). 3—Whey proteins. In G. O. Phillips & P. A. Williams (Éds.), *Handbook of Food Proteins* (p. 30-55). Woodhead Publishing. <https://doi.org/10.1533/9780857093639.30>
- Bouman, S., Brinkman, D. W., Jong, P. de, & Waalewijn, R. (1988). Multistage evaporation in the dairy industry: Energy savings, product losses, and cleaning. *Preconcentration and Drying of Food Materials: Thijssen Memorial Symposium: Proc of the International Symposium on Preconcentration and Drying of Foods, Eindhoven, The Netherlands, Nov 5-6, 1987 / Edited by S. Bruin*, 51-60.
- Chandra, N., Brew, K., & Acharya, K. R. (1998). Structural Evidence for the Presence of a Secondary Calcium Binding Site in Human α -Lactalbumin, *Biochemistry*, 37(14), 4767-4772. <https://doi.org/10.1021/bi973000t>
- Chrysina, E. D., Brew, K., & Acharya, K. R. (2000). Crystal Structures of Apo- and Holo-bovine α -Lactalbumin at 2.2-Å Resolution Reveal an Effect of Calcium on Inter-lobe Interactions*. *Journal of Biological Chemistry*, 275(47), 37021-37029. <https://doi.org/10.1074/jbc.M004752200>
- Connell, J. E., & Fox, P. F. (2001). Effect of beta-lactoglobulin and precipitation of calcium phosphate on the thermal coagulation of milk. *The Journal of Dairy Research*, 68(1), 81-94. <https://doi.org/10.1017/s0022029900004556>
- De Wit, J. N. (1990). Thermal Stability and Functionality of Whey Proteins. *Journal of Dairy Science*, 73(12), 3602-3612. [https://doi.org/10.3168/jds.S0022-0302\(90\)79063-7](https://doi.org/10.3168/jds.S0022-0302(90)79063-7)
- Dehbani, M., & Rahimi, M. (2018). Introducing ultrasonic falling film evaporator for moderate temperature evaporation enhancement. *Ultrasonics Sonochemistry*, 42, 689-696. <https://doi.org/10.1016/j.ultsonch.2017.12.016>
- de Wit, J. N. (2009). Thermal behavior of bovine β -lactoglobulin at temperatures up to 150°C. a review. *Trends in Food Science & Technology*, 20(1), 27-34. <https://doi.org/10.1016/j.tifs.2008.09.012>

- Dunna, V., & Srinivas Kishore, P. (2015). *Thermal Analysis on Triple Effect Falling Film Evaporator*. 03, 391-394.
- Dunstan, D. E., Hamilton-Brown, P., Asimakis, P., Ducker, W., & Bertolini, J. (2009). Shear-induced structure and mechanics of β -lactoglobulin amyloid fibrils. *Soft Matter*, 5(24), 5020-5028. <https://doi.org/10.1039/B914089A>
- Fernandes, S., Gomes, I. B., Simões, L. C., & Simões, M. (2021). Overview of the hydrodynamic conditions found in industrial systems and their impact in (bio)fouling formation. *Chemical Engineering Journal*, 418, 129348. <https://doi.org/10.1016/j.cej.2021.129348>
- Fickak, A., Al-Raisi, A., & Chen, X. D. (2011). Effect of whey protein concentration on the fouling and cleaning of a heat transfer surface. *Journal of Food Engineering*, 104(3), 323-331. <https://doi.org/10.1016/j.jfoodeng.2010.11.004>
- Fox, P. F. (2003). 2—The major constituents of milk. In G. Smit (Éd.), *Dairy Processing* (p. 5-41). Woodhead Publishing. <https://doi.org/10.1533/9781855737075.1.5>
- Garrett-Price, B. A., Smith, S. A., & Watts, R. L. (1984). *Industrial fouling: Problem characterization, economic assessment, and review of prevention, mitigation, and accommodation techniques* (PNL-4883, 5310685; p. PNL-4883, 5310685). <https://doi.org/10.2172/5310685>
- Geurts, P. W., Pieter Walstra, Jan T. M. Wouters, Tom J. (2005). *Dairy Science and Technology* (2^e éd.). CRC Press. <https://doi.org/10.1201/9781420028010>
- Gillham, C. R., Fryer, P. J., Hasting, A. P. M., & Wilson, D. I. (2000). Enhanced cleaning of whey protein soils using pulsed flows. *Journal of Food Engineering*, 46(3), 199-209. [https://doi.org/10.1016/S0260-8774\(00\)00083-2](https://doi.org/10.1016/S0260-8774(00)00083-2)
- Gulzar, M., Bouhallab, S., Jeantet, R., Schuck, P., & Croguennec, T. (2011). Influence of pH on the dry heat-induced denaturation/aggregation of whey proteins. *Food Chemistry*, 129(1), 110-116. <https://doi.org/10.1016/j.foodchem.2011.04.037>
- Hagsten, C., Altskar, A., Gustafsson, S., Loren, N., Hamberg, L., Innings, F., Paulsson, M., & Nylander, T. (2016). Composition and structure of high-temperature dairy fouling. *Food Structure-Netherlands*, 7, 13-20. <https://doi.org/10.1016/j.foostr.2015.12.002>
- Indyk, H. E., Hart, S., Meerkerk, T., Gill, B. D., & Woollard, D. C. (2017). The β -lactoglobulin content of bovine milk: Development and application of a biosensor immunoassay. *International Dairy Journal*, 73, 68-73. <https://doi.org/10.1016/j.idairyj.2017.05.010>
- Jebson, S., Chen, H., & Campanella, O. (2009). Fouling in a Centritherm Evaporator with Whey Solutions. *Heat Transfer Engineering*, 30(10-11), 859-867. <https://doi.org/10.1080/01457630902753722>
- Jeurnink, T., & Dekruif, K. (1995). Calcium-Concentration in Milk about Heat-Stability and Fouling. *Netherlands Milk and Dairy Journal*, 49(2-3), 151-165.
- Kannan, M. (2018). *Scanning Electron Microscopy: Principle, Components and Applications* (p. 81-92).
- Kontopidis, G., Holt, C., & Sawyer, L. (2004). Invited review: Beta-lactoglobulin: binding properties, structure, and function. *Journal of Dairy Science*, 87(4), 785-796. [https://doi.org/10.3168/jds.S0022-0302\(04\)73222-1](https://doi.org/10.3168/jds.S0022-0302(04)73222-1)
- Kukulka, D. J., BAIER, R. E., & MOLLENDORF, J. C. (2004). Factors Associated with Fouling in the Process Industry. *Heat Transfer Engineering*, 25(5), 23-29. <https://doi.org/10.1080/01457630490458978>
- Lam, R. S. H., & Nickerson, M. T. (2015). The effect of pH and temperature pre-treatments on the structure, surface characteristics and emulsifying properties of alpha-lactalbumin. *Food Chemistry*, 173, 163-170. <https://doi.org/10.1016/j.foodchem.2014.09.078>
- Lefèvre, T., & Subirade, M. (2000). Molecular differences in the formation and structure of fine-stranded and particulate beta-lactoglobulin gels. *Biopolymers*, 54(7), 578-586. [https://doi.org/10.1002/1097-0282\(200012\)54:7<578 : AID-BIP100>3.0.CO ;2-2](https://doi.org/10.1002/1097-0282(200012)54:7<578 : AID-BIP100>3.0.CO ;2-2)
- Mehalebi, S., Nicolai, T., & Durand, D. (2008). Light scattering study of heat-denatured globular protein aggregates. *International Journal of Biological Macromolecules*, 43(2), 129-135. <https://doi.org/10.1016/j.ijbiomac.2008.04.002>
- Mercadante, D., Melton, L. D., Norris, G. E., Loo, T. S., Williams, M. A. K., Dobson, R. C. J., & Jameson, G. B. (2012). Bovine β -Lactoglobulin Is Dimeric Under Imitative Physiological

- Conditions: Dissociation Equilibrium and Rate Constants over the pH Range of 2.5–7.5. *Biophysical Journal*, 103(2), 303-312. <https://doi.org/10.1016/j.bpj.2012.05.041>
- Moakes, R. J. A., Sullo, A., & Norton, I. T. (2015). Preparation and characterization of whey protein fluid gels: The effects of shear and thermal history. *Food Hydrocolloids*, 45, 227-235. <https://doi.org/10.1016/j.foodhyd.2014.11.024>
- Mura, E., & Gourdon, M. (2016). Interfacial shear stress, heat transfer and bubble appearance in falling film evaporation. *Experimental Thermal and Fluid Science*, 79, 57-64. <https://doi.org/10.1016/j.expthermflusci.2016.06.027>
- Paramalingam, S., Winchester, J., & Marsh, C. (2000). On the fouling of falling film evaporators due to film break-up. *Food and Bioprocess Processing*, 78(C2), 79-84. <https://doi.org/10.1205/096030800532770>
- Pereira, P. C. (2014). Milk nutritional composition and its role in human health. *Nutrition*, 30(6), 619-627. <https://doi.org/10.1016/j.nut.2013.10.011>
- Piepiorka-Stepuk, J., Tandecka, K., & Jakubowski, M. (2016). An Analysis of Milk Fouling Formed During Heat Treatment on a Stainless-Steel Surface with Different Degrees of Roughness. *Czech Journal of Food Sciences*, 34(3), 271-279. <https://doi.org/10.17221/466/2015-CJFS>
- Rahaei, N., Nasr, M., & Reza, M. (2019). Improving Heat Transfer in Falling Film Evaporators in Food Industries. *Iranian Journal of Chemistry & Chemical Engineering-International English Edition*, 38, 237. <https://doi.org/10.30492/IJCCE.2020.43322>
- Relkin, P. (1996). Thermal unfolding of beta-lactoglobulin, alpha-lactalbumin, and bovine serum albumin. A thermodynamic approach. *Critical Reviews in Food Science and Nutrition*, 36(6), 565-601. <https://doi.org/10.1080/10408399609527740>
- Roefs, S. P., & De Kruif, K. G. (1994). A model for the denaturation and aggregation of beta-lactoglobulin. *European Journal of Biochemistry*, 226(3), 883-889. <https://doi.org/10.1111/j.1432-1033.1994.00883.x>
- Scott, S. A., Brooks, J. D., Rakonjac, J., Walker, K. M. R., & Flint, S. H. (2007). The formation of thermophilic spores during the manufacture of whole milk powder. *International Journal of Dairy Technology*, 60(2), 109-117. <https://doi.org/10.1111/j.1471-0307.2007.00309.x>
- Shah, F., Ruscak, K., & Palmquist, A. (2019). 50 years of scanning electron microscopy of bone—A comprehensive overview of the important discoveries made and insights gained into bone material properties in health, disease, and taphonomy. *Bone Research*, 7. <https://doi.org/10.1038/s41413-019-0053-z>
- Shimada, K., & Cheftel, J. C. (1988). Texture characteristics, protein solubility, and sulfhydryl group/disulfide bond contents of heat-induced gels of whey protein isolate. *Journal of Agricultural and Food Chemistry*, 36(5), 1018-1025. <https://doi.org/10.1021/jf00083a029>
- Silva, N. N., Piot, M., de Carvalho, A. F., Violleau, F., Fameau, A.-L., & Gaucheron, F. (2013). PH-induced demineralization of casein micelles modifies their physico-chemical and foaming properties. *Food Hydrocolloids*, 32(2), 322-330. <https://doi.org/10.1016/j.foodhyd.2013.01.004>
- Simmons, M. J. H., Jayaraman, P., & Fryer, P. J. (2007). The effect of temperature and shear rate upon the aggregation of whey protein and its implications for milk fouling. *Journal of Food Engineering*, 79(2), 517-528. <https://doi.org/10.1016/j.jfoodeng.2006.02.013>
- Smirnova, A., Konoplev, G., Mukhin, N., Stepanova, O., & Steinmann, U. (2020). Milk as a Complex Multiphase Polydisperse System: Approaches for the Quantitative and Qualitative Analysis. *Journal of Composites Science*, 4(4), 151.
- Tanford, C., Bunville, L. G., & Nozaki, Y. (1959). The Reversible Transformation of β -Lactoglobulin at pH 7.51. *Journal of the American Chemical Society*, 81(15), 4032-4036. <https://doi.org/10.1021/ja01524a054>
- Tolkach, A., & Kulozik, U. (2007). Reaction kinetic pathway of reversible and irreversible thermal denaturation of beta-lactoglobulin. *Le Lait*, 87(4-5), 301-315. <https://doi.org/10.1051/lait:2007012>
- Vilotte, A. (2021). *Aggregation, gelation, and hydrodynamic spinning of whey proteins*. Université Grenoble Alpes.

- Walkenström, P., Windhab, E., & Hermansson, A.-M. (1998). Shear-induced structuring of particulate whey protein gels. *Food Hydrocolloids*, 12(4), 459-468. [https://doi.org/10.1016/S0268-005X\(98\)00064-2](https://doi.org/10.1016/S0268-005X(98)00064-2)
- Walstra, P., Walstra, P., Wouters, J. T. M., & Geurts, T. J. (2005). *Dairy Science and Technology* (2^e éd.). CRC Press. <https://doi.org/10.1201/9781420028010>
- Wilson, D. I. (2018). Fouling during food processing – progress in tackling this inconvenient truth. *Current Opinion in Food Science*, 23, 105-112. <https://doi.org/10.1016/j.cofs.2018.10.002>
- Wolz, M., Mersch, E., & Kulozik, U. (2016). Thermal aggregation of whey proteins under shear stress. *Food Hydrocolloids*, 56, 396-404. <https://doi.org/10.1016/j.foodhyd.2015.12.036>
- Yagi, M., Sakurai, K., Kalidas, C., Batt, C. A., & Goto, Y. (2003). Reversible Unfolding of Bovine β -Lactoglobulin Mutants without a Free Thiol Group *. *Journal of Biological Chemistry*, 278(47), 47009-47015. <https://doi.org/10.1074/jbc.M308592200>
- Zhang, Y., Munir, M. T., Udugama, I., Yu, W., & Young, B. R. (2018). Modeling of a milk powder falling film evaporator for predicting process trends and comparison of energy consumption. *Journal of Food Engineering*, 225, 26-33. <https://doi.org/10.1016/j.jfoodeng.2018.01.016>
- Zhou, W., Apkarian, R., Wang, Z., & Joy, D. (2006). *Fundamentals of Scanning Electron Microscopy (SEM)* (p. 1-40). https://doi.org/10.1007/978-0-387-39620-0_1